JOURNAL OF PETROLOGY | VOLUME 48 | NUMBER 6 | PAGES 1155–1183 | 2007 | doi:10.1093/petrology/egm013

Constraining Fluid and Sediment Contributions to Subduction-Related Magmatism in Indonesia: Ijen Volcanic Complex

H. K. HANDLEY[1]*, C. G. MACPHERSON[1], J. P. DAVIDSON[1], K. BERLO[2] AND D. LOWRY[3]

[1]DEPARTMENT OF EARTH SCIENCES, DURHAM UNIVERSITY, DURHAM DH1 3LE, UK

[2]DEPARTMENT OF EARTH SCIENCES, BRISTOL UNIVERSITY, BRISTOL BS8 1RJ, UK

[3]DEPARTMENT OF GEOLOGY, ROYAL HOLLOWAY UNIVERSITY OF LONDON, EGHAM TW20 0EX, UK

RECEIVED JULY 10, 2006; ACCEPTED MARCH 7, 2007
ADVANCE ACCESS PUBLICATION APRIL 17, 2007

Ijen Volcanic Complex (IVC) in East Java, Indonesia is situated on thickened oceanic crust within the Quaternary volcanic front of the Sunda arc. The 20 km wide calderas complex contains around 22 post-caldera eruptive centres, positioned either around the caldera-rim (CR) or along a roughly NE–SW lineament inside the caldera (IC). The CR and IC lavas exhibit separate differentiation histories. Major element and trace element modelling shows that fractionation of olivine, clinopyroxene, Fe–Ti oxide ± plagioclase is important in the CR group, whereas plagioclase is the dominant fractionating mineral in the same assemblage for the IC group. Spatial controls on magmatic differentiation highlight important structural controls on magma storage and ascent at IVC. Mantle-like $\delta^{18}O$ values, restricted ranges in Sr, Nd and Hf isotope ratios, and a lack of correlation between isotope ratios and indices of differentiation in IVC lavas are consistent with magmatic evolution through fractional crystallization. Furthermore, the small ranges in isotopic ratios throughout the complex indicate little heterogeneity in the mantle. IVC lavas possess higher $^{176}Hf/^{177}Hf$ and $^{143}Nd/^{144}Nd$ isotope ratios than other volcanoes of Java, representing the least contaminated source so far analysed and, therefore, give the best estimate yet of the pre-subduction mantle wedge isotopic composition beneath Java. Trace element and radiogenic isotope data are consistent with a two-stage, three-component petrogenetic model for IVC, whereby an Indian-type mid-ocean ridge basalt (I-MORB)-like fertile mantle wedge is first infiltrated by a small percentage of fluid, sourced from the altered oceanic crust, prior to addition of <1% Indian Ocean sediment dominated by pelagic material.

KEY WORDS: *differentiation; geochemistry; source components; Sr, Nd, Hf and O isotopes; Sunda arc*

INTRODUCTION AND SETTING

Understanding magma genesis and evolution in subduction zone environments is crucial to understanding the formation of the continents and crustal recycling in the mantle. However, determining original source compositions of volcanic arc rocks can be challenging, as lavas rarely reach the Earth's surface without experiencing some processes that modify their composition; for example, crystal fractionation, magma mixing or crustal contamination (Davidson, 1996; Thirlwall *et al.*, 1996; Mandeville *et al.*, 1996; Reubi & Nicholls, 2004; Davidson *et al.*, 2005). In most petrogenetic models, island arc magmas originate from a mantle wedge that is modified by slab-derived components (Hawkesworth *et al.*, 1991; McCulloch & Gamble, 1991; Pearce & Peate, 1995). The magnitude and nature of the contribution from the subducting slab is debated, although there is a consensus that a slab-derived fluid is involved, consisting of fluids from either the altered oceanic crust (Hawkesworth *et al.*, 1997; Turner *et al.*, 1997; Turner & Foden, 2001) or overlying sediments (Class *et al.*, 2000), and other components, possibly partial melts, derived from subducted sediment (Edwards *et al.*, 1993; Elliott *et al.*, 1997; Turner & Foden, 2001; Vroon *et al.*, 2001).

*Corresponding author. Present address: GEMOC Key Centre, Department of Earth and Planetary Sciences, Macquarie University, Sydney, NSW 2109, Australia. Telephone: +61 2 9850 4405. Fax: +61 2 9850 8943. E-mail: hhandley@els.mq.edu.au

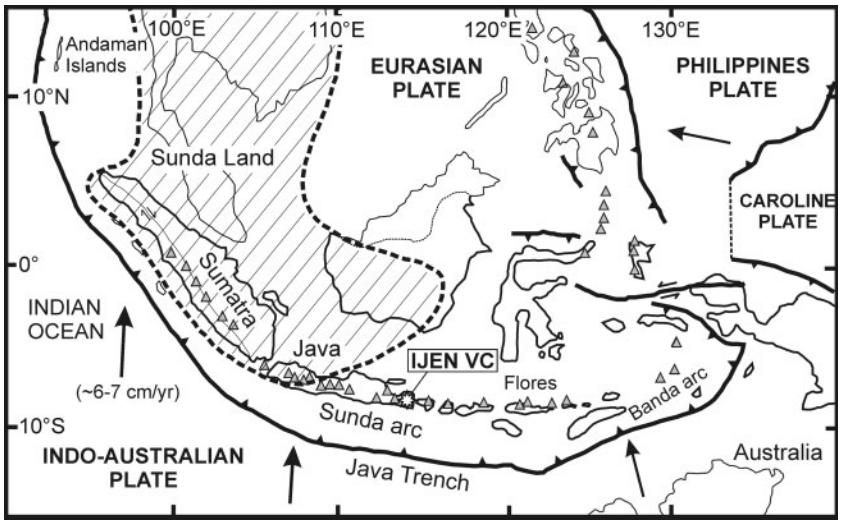

Fig. 1. Tectonic setting of Indonesia [modified from Hoffmann-Rothe *et al.* (2001)], showing the location of Ijen Volcanic Complex (open star). Black arrows represent the directions of plate movement. Convergence rate of the Indo-Australian Plate and Eurasian Plate from Chase (1978), DeMets *et al.* (1990) and Tregoning *et al.* (1994). Grey triangles indicate active volcanoes. Dashed outline of 'Sunda Land' indicates possible extent of continental lithospheric basement (Hamilton, 1979).

Ijen volcanic complex (IVC) is located on the eastern edge of Java within the Quaternary volcanic front of the Sunda arc (Fig. 1). The arc forms the western part of the Indonesian subduction zone system, which extends over 3000 km from the Andaman Islands north of Sumatra to Flores in the Banda Sea. It formed as a result of the northward subduction of the Indo-Australian Plate beneath the Eurasian Plate at a rate of around 6–7 cm/year (DeMets *et al.*, 1990; Tregoning *et al.*, 1994). Despite this apparently simple tectonic setting, understanding magma genesis and evolution at the Sunda arc is complicated by the variable nature of the arc crust, the changing age of the subducting oceanic crust, which increases eastwards from ~80 to ~130 Ma (Plank & Langmuir, 1998), and variation in the type and amount of subducted sediment, which ranges from bimodal siliceous ooze and clays with minor turbidites beneath the western part of the arc to strongly clay-dominated material with secondary carbonate and minor siliceous ooze in the east (Plank & Langmuir, 1998). Along the length of the arc the composition and thickness of the overriding Eurasian plate is also thought to change, from continental in the west to oceanic in the east (Hamilton, 1979). Beneath Java, the crust is ~20 km thick and has a seismic velocity structure intermediate between continental and oceanic (Whitford, 1975). The Java crust is said to consist of ophiolite slivers, mélange and older volcanic rocks (Hamilton, 1979). The Sunda Land (SE Asian continental part of the Sunda block–Eurasian plate with pre-Tertiary basement) boundary shown in Fig. 1 suggests that in western Java the island arc is built on continental material. In eastern Java beneath the IVC (outside the hypothesized Sunda Land boundary) the overriding plate comprises thickened oceanic crust. However, recent research on inherited zircons (Smyth, 2005) provides evidence for old continental basement beneath the Southern Mountains Arc (south of the active volcanic axis) in East Java.

Despite a number of petrogenetic studies of Javan volcanoes (Edwards *et al.*, 1993; Turner & Foden, 2001; Gertisser & Keller, 2003; and references therein), uncertainty still prevails over the nature of the subduction component and the mechanisms by which it is added to the mantle wedge. For example, Edwards *et al.* (1993) proposed a homogeneous slab contribution along the Sunda arc, whereas Turner & Foden (2001) identified along-arc heterogeneity in this component. The IVC is located on the eastern edge of Java within the Quaternary volcanic front of the Sunda arc (Fig. 1) and is therefore in an ideal location to investigate the mantle source composition beneath Java; the relatively thin crust on which the volcano sits minimizes the likelihood of high-level continental crust contamination (compared with studies in West Java) and potentially allows us to constrain better crustal contributions in the mantle source. Furthermore, apparent spatial controls on some major and trace element variations at IVC mean that the volcanic complex provides a useful opportunity to investigate the relationship between volcanic structure and shallow-level processes influencing the composition of arc lavas. The aims of this study are, therefore, two-fold: (1) to identify the impact, if any, of volcanic and subjacent structure upon magmatic differentiation; (2) to characterize the IVC magma source and place constraints on

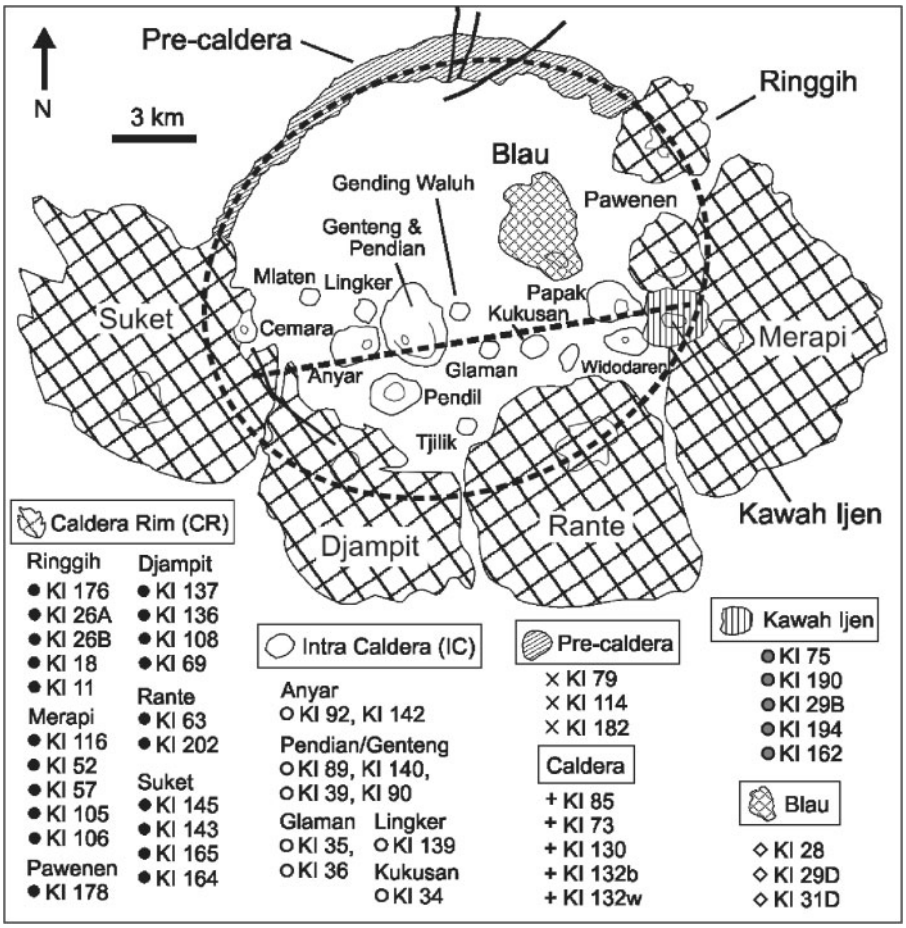

Fig. 2. Schematic map of the IVC showing the geographical relationships of the eruptive centres. Oval dashed line denotes the caldera rim (hypothesized in the south). Straight dashed line represents the lineation of intra-caldera volcanoes [based on Berlo (2001)]. Continuous black lines in the north and SW indicate faults. Volcano boundaries represent the obvious topographic control exerted by the post-caldera volcanic centres. The general provenance of the samples used in this study is indicated below the map; corresponding data symbols used in subsequent figures are shown. [Sample grid references from Sitorus (1990) are given in Electronic Appendix 1.]

the nature of the slab component(s) and the transfer mechanism(s) to the mantle wedge.

OVERVIEW OF THE IJEN VOLCANO COMPLEX

The Ijen volcanic complex consists of several stratovolcanoes and cinder cones constructed within and around a 20 km wide caldera (Fig. 2). The complex takes its name from Kawah Ijen volcano, the only volcano of the complex that is currently active. Based on an episode of caldera collapse, the stratigraphic succession has been divided into pre-caldera, caldera and post-caldera groups (van Bemmelen, 1949). Little is known about the age, structure or volcanic history of the pre-caldera cone (Old Ijen); it is thought to be either early (van Bemmelen, 1949) or late (Sitorus, 1990; K–Ar dating) Pleistocene. Sitorus (1990) considered the pre-caldera volcanic structure to be a large, single, composite volcano whereas Berlo (2001), suggested that the pre-caldera collapse volcano may have had multiple vents. Kemmerling (1921) has suggested the possibility that twin volcanoes made up Old Ijen, because of the oval shape of the subsequent caldera. The deposits of Old Ijen disconformably overlie Miocene limestone (van Bemmelen, 1949) and consist of pyroclastic flow deposits, a series of pumice airfall deposits and several lava flows. The caldera wall forms a prominent arcuate ridge in the north, but elsewhere in the complex the caldera rim is buried by the post-caldera volcanoes (Fig. 2). The collapse of the pre-caldera cone(s) is thought to have occurred in stages more than 50 000 years ago (Sitorus, 1990). The caldera group consists of two main units, comprising large volumes of caldera-forming ignimbrite and minor layers of pumice airfall and lahar deposits. Most of the eruptive products were deposited to the north (van Bemmelen, 1949). Shortly after caldera collapse a resurgent dome (Blau)

formed inside the caldera. The post-caldera group is characterized by many types of eruption (phreatomagmatic, phreatic, strombolian and plinian) and comprises 58 lithological volcanic units, erupted from 22 separate vents (Sitorus, 1990). The post-caldera eruptive centres can be further divided on the basis of their geographical position within the complex: those located on the caldera rim (CR), dominantly composite cones, or intra-caldera (IC) centres situated inside the southern part of the caldera along a ENE–WSW lineation (Fig. 2). The latter are predominantly cinder cones with minor composite cones and a lava dome. The IC volcanoes are generally younger (with the exception of Blau) than the CR volcanoes (Sitorus, 1990; Berlo, 2001). Faulting is evident within the caldera complex in the north (Fig. 2) and large faults have affected the caldera-rim volcanoes of Merapi, Ringgih and Djampit. Present volcanic activity is limited to Ijen crater (Kawah Ijen), an acidic crater lake with a maximum diameter of 1·2 km and a depth of around 200–300 m. The last major eruption created phreatomagmatic air fall and pyroclastic flow deposits ~2590 years ago. Historical eruptions, which were mainly phreatic, occurred in 1796, 1817, 1917, 1936, 1952, 1993, 1994, 1999 and 2000 (Volcanic Survey of Indonesia: http://www.vsi.esdm.go.id/volcanoes/ijen/history.html).

SAMPLE GROUPINGS

This study builds on the established stratigraphy and preliminary geochemical work of Sitorus (1990). Few samples were available from the pre-caldera and caldera groups, therefore emphasis is on the geochemistry of the post-caldera rocks. Based on temporal variations in geochemistry, particularly in SiO_2, FeO, CaO, Ni and Sr contents, Sitorus (1990) divided the post-caldera samples into six groups, but admitted that the variations are not entirely consistent through time, either within or between groups. Therefore, in this study the majority of the samples have been simply divided into CR and IC groups, based on their spatial distribution rather than age (Fig. 2). The centres of Kawah Ijen and Blau are considered separately from the two main post-caldera groups. Kawah Ijen is located on the western flank of Merapi (a CR volcano) in line with the other intra-caldera centres and appears to have geochemical affinities to both groups. Blau, although easily identifiable as a volcanic centre inside the caldera, is located north of the linear trend of the other intra-caldera volcanoes and geochemical data show scatter between the two groups. Stratigraphic relationships, geomorphology (deep incised valleys) and K–Ar dating suggest that Blau is significantly older than the rest of the intra-caldera centres (Sitorus, 1990).

A total of 43 samples from the IVC were obtained from the collection of Sitorus (1990) as rock powders, with the exception of five samples, for which hand specimens were also obtained. Major element data, mineralogical data and petrographic descriptions of the IVC rocks are taken from Sitorus (1990) and presented in Electronic Appendices 1–3, respectively (which may be downloaded from the *Journal of Petrology* website at http://petrology.oxfordjournals.org).

ANALYTICAL TECHNIQUES

Five bulk-rock and 43 powdered samples were available for trace element and isotopic study. The generally low range of loss on ignition values (0·39–1·25 wt %) for the post-caldera rocks with the exception of three samples (2·24, 2·26 and 4·39 wt % LOI) indicates that most of the samples are fresh. Four of the five caldera samples with reported major element data (Electronic Appendix 1) have high LOI values and were not considered suitable for trace element and isotopic analysis.

Trace element concentrations in 43 IVC rocks were determined using a PerkinElmer ELAN 6000 quadrupole inductively coupled plasma mass spectrometry (ICP-MS) system at Durham University. Full details of the analytical procedure and instrument operating conditions have been given by Ottley *et al.* (2003) and Handley (2006). Calibration of the ELAN was achieved via the use of in-house standards and international reference materials [W2, BHVO-1, AGV1, BE-N and BIR1, using the accepted standard values given by Potts *et al.* (1992)], together with procedural blanks (three per batch). Internal and external reproducibility of standard values are generally less than 3% relative standard deviation (Ottley *et al.*, 2003). Comparison of Zr and Ti elemental concentrations in IVC rocks obtained by X-ray fluorescence (Sitorus, 1990) and ICP-MS (this study) show excellent agreement, with mean relative differences of 6% and 7%, respectively.

Sr, Nd and Hf isotope analysis was undertaken at the Arthur Holmes Isotope Geology Laboratory (AHIGL), Durham University. The sample dissolution procedure and separation of Hf and Nd from rock samples is based on that presented by Dowall *et al.* (2003). The chemical separation procedure for Sr in this study follows that outlined by Charlier *et al.* (2006). Sr, Nd and Hf fractions were measured for isotope ratios using the AHIGL ThermoElectron Neptune multi-collector ICP-MS system. Detailed instrument operating conditions (including cup configurations and interference corrections) have been given by Dowall *et al.* (2003) and Nowell *et al.* (2003). Samples were analysed on several separate occasions. Data quality was monitored over the separate sessions by frequent analysis of standard reference materials throughout each run. Measured values for the NBS 987, J&M and JMC 475 standards ± 2SD error over the period of study were 0·710262 ± 11 ($n = 53$), 0·511106 ± 10 ($n = 74$) and 0·282146 ± 4 ($n = 51$), respectively. Data are

plotted relative to NBS 987, J&M and JMC 475 standard values of 0·71024 (Thirlwall, 1991), 0·511110 (Royse *et al.*, 1998) and 0·282160 (Nowell *et al.*, 1998), respectively. Total procedural blanks for Sr, Nd and Hf were determined by ICP-MS on the PerkinElmer ELAN 6000 quadrupole ICP-MS system at Durham University and were below 1·2 ng for Sr, 219 pg for Nd and 73 pg for Hf. These values are considered insignificant in relation to the quantity of Sr, Nd and Hf typically processed from IVC rocks (~12 μg, 3 μg and 500 ng, respectively).

Oxygen isotope analyses of mineral separates were performed by laser-fluorination at Royal Holloway, University of London using the procedures outlined by Macpherson *et al.* (2000). Oxygen results are reported as per mil deviations relative to the standard mean ocean water (SMOW) standard. In-house standard values of SC olivine 2 and GMG II over the period of study were +5·24‰ ± 0·04 (1σ, $n = 6$) and +5·69‰ ± 0·08 (1σ, $n = 15$); within 0·01‰ of accepted values. Precision and accuracy within runs were similar to the overall standard results. Oxygen yields were greater than 98% for olivine, 93% for plagioclase and between 92 and 94% for clinopyroxene. Although the yields for plagioclase and clinopyroxene are slightly low, they were consistent over the three sessions. Replicate analyses of olivine, plagioclase and clinopyroxene were within 0·06‰, 0·09‰ and 0·04‰, respectively.

GEOCHEMISTRY

Major element data

Major element data are reported in Electronic Appendix 1 and illustrated in Fig. 3. Although SiO_2 is commonly used as the index of differentiation for typically evolved arc lavas (Davidson *et al.*, 2005), MgO was chosen here as (1) IVC includes a large number of relatively less evolved ($SiO_2 < 55$ wt %) rocks, and (2) there appears to be some division in SiO_2 contents between the CR and IC post-caldera groups at lower MgO content (Fig. 3a). Lavas from IVC display a broad range in SiO_2 content from 48 to 63 wt % and relatively low MgO contents (<5·8 wt %) typical of island arc volcanoes, which suggests that no true, primary basalts were erupted within the complex. MgO correlates positively with Fe_2O_3, TiO_2 and CaO, whereas Na_2O, SiO_2 and K_2O generally increase with decreasing MgO. Al_2O_3 and P_2O_5 data are considerably more scattered, especially at lower MgO contents (Fig. 3).

The IC samples form a coherent, linear array in the majority of variation diagrams, with a narrower range of SiO_2 and MgO than for the CR volcanic rocks. IC and CR rocks generally appear to follow different trends on plots of SiO_2, Al_2O_3, K_2O and CaO against MgO (Fig. 3a–d), with the exception of four CR samples (KI 202, KI 136, KI 164 and KI 108) that follow the IC trend. The IC group has higher SiO_2 and K_2O contents than the CR group at similar MgO and displays strong negative correlations, whereas within the CR group there is a weaker and less obviously negative correlation between SiO_2 and K_2O and MgO (Fig. 3a and c). The more differentiated CR rocks (below ~4 wt % MgO) have elevated CaO and Al_2O_3 contents when compared with the IC samples at the same degree of differentiation (Fig. 3b and d). Samples from Kawah Ijen and Blau appear to straddle the two trends in the majority of the variation diagrams (e.g. Fig. 3b–d).

Trace element geochemistry

Ni (<40 ppm) and Cr (<60 ppm) concentrations are low in IVC rocks (Table 1) and Ni is positively correlated with MgO (e.g. Fig. 4). There is a large decrease in Ni (and Cr) abundance from the most mafic rocks to those with intermediate MgO contents, whereas the more evolved lavas display more constant concentrations. Large ion lithophile element (LILE; Rb, Cs, Ba and including U and Th) concentrations (e.g. Fig. 4b and c) generally increase with decreasing MgO. Variation of Rb with MgO mirrors that of K_2O (Fig. 3c), where IC group contents are higher than the relatively constant concentrations in the CR group. Sr concentrations, on the other hand, are more elevated in the CR group and generally increase with decreasing MgO, whereas Sr concentrations in the IC rocks are in the main lower at similar MgO (Fig. 4d); Al_2O_3 and CaO exhibit similar behaviour. The IC samples have higher abundances of high field strength elements (HFSE), such as Zr, Hf, Nb and Ta, than the CR rocks at a given MgO (Fig. 4e and f). The variation of these elements also mirrors that of K_2O. Rare earth element (REE) variation with MgO is illustrated in Fig. 4g and h. Light REE (LREE, e.g. La) concentrations in the IVC rocks generally increase with decreasing MgO (Fig. 4g); however, heavy REE (HREE) variation trends are more difficult to discern; there is a wide variation in Yb at low MgO content (Fig. 4h).

Mid-ocean ridge basalt (MORB)-normalized trace element abundance patterns (Fig. 5) are typical of island arc volcanoes, with enrichment of the more mobile LILE and LREE relative to HFSE and HREE. The highly to moderately incompatible elements are all enriched relative to MORB, similar to those from other Sunda arc volcanoes (Turner & Foden, 2001) and local sediments (Vroon *et al.*, 1995). The IC group are generally more enriched than the CR group. This enrichment is emphasized in the inset diagram of Fig. 5, where the IC are normalized to the CR group. There is a general decrease in the degree of enrichment of the IC as element incompatibility decreases, with the exception of Ba and Sr, which are considerably less enriched relative to their neighbouring elements, and in the case of Sr, which is actually depleted relative

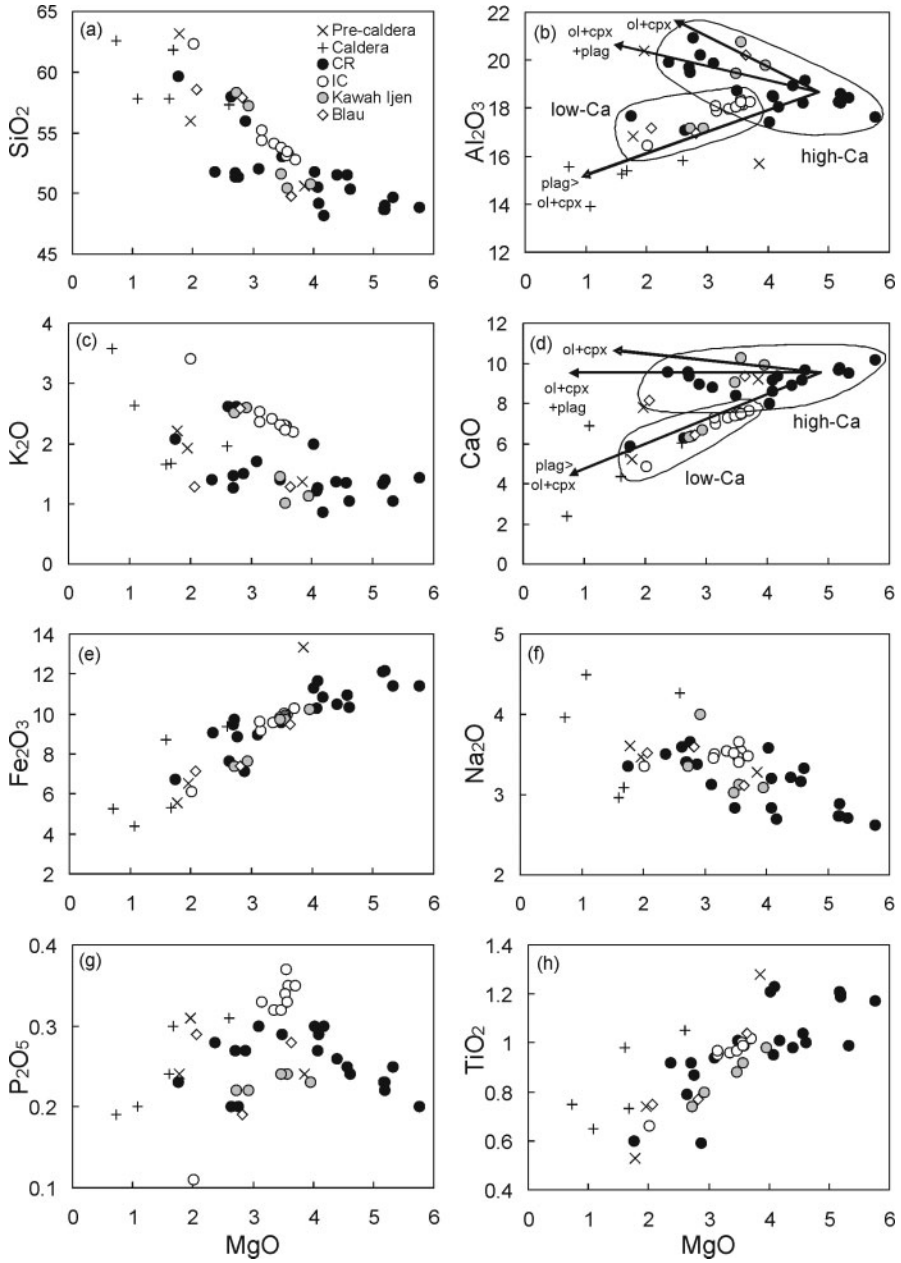

Fig. 3. Major element variation diagrams for IVC rocks separated by geographical group. Black arrows in (b) and (d) are general crystallization vectors indicating the expected direction of magmatic evolution with the crystallization of varying amounts of olivine (ol), clinopyroxene (cpx) and plagioclase (plag). Vectors were calculated from averaged microprobe mineral data (Sitorus, 1990). The major element data are from Sitorus (1990) (see Electronic Appendix 1). Fields indicate differences between the two main groups; high Ca (largely CR) and low Ca (largely IC) at IVC.

to the CR group. There is greater enrichment of Zr and Hf in the IC group compared with the more compatible elements, whereas the Ti concentrations of the IC and CR rocks are identical.

Radiogenic isotopes

The Sr–Nd–Hf isotope compositions of the IVC samples are listed in Table 1 and plotted in Fig. 6. In contrast to their major and trace element compositions, the intracaldera and caldera-rim groups cannot be distinguished from one another on the basis of radiogenic isotopes. The relatively large dataset displays a restricted range in $^{87}Sr/^{86}Sr$ (0·704169–0·704483), $^{143}Nd/^{144}Nd$ (0·512814–0·512895) and $^{176}Hf/^{177}Hf$ (0·283078–0·283133), and plots within the range of other Indonesian island arc volcanoes. The Sr and Nd isotope ratios of lavas from the

Table 1: Trace element and Sr–Nd–Hf isotope data for IVC volcanic rocks

	Pre-caldera			Caldera	Post-caldera Caldera-rim (CR)									
					Djampit	Djampit	Djampit	Djampit	Ringgih	Ringgih	Ringgih	Ringgih	Ringgih	Pawenen
	KI 79	KI 114	KI 182	KI 85	KI 108	KI 69	KI 137	KI 136	KI 11	KI 26A	KI 26B	KI 18	KI 176	KI 178
Sc	37	12	11	24	31	38	18	10	32	19	19	20	27	25
Ti	8260	4585	3291	6911	8134	7768	6114	3830	6384	5694	5005	5694	5359	8014
V	462	95	95	176	333	418	199	89	381	217	217	222	279	241
Cr	0·0	0·4	4·3	1·1	0·9	59·4	1·1	1·4	4·5	0·0	0·3	-0·2	18·2	1·3
Co	58	31	32	51	207	55	35	24	46	32	37	35	33	36
Ni	8·3	2·6	3·8	10·7	10·8	37·8	7·1	2·7	23·3	4·8	4·0	4·5	14·6	4·3
Cu	233	42	24	43	181	175	34	24	198	125	123	113	74	52
Zn	111	73	62	115	101	85	106	89	86	77	73	75	74	98
Ga	20	20	17	21	21	19	20	19	19	18	18	18	18	19
Rb	27·4	45·1	61·9	43·1	57·7	38·5	28·4	60·3	31·9	27·0	25·0	27·2	17·8	19·4
Sr	517	575	547	484	487	491	501	485	500	654	626	640	567	612
Y	30	28	20	35	31	25	30	39	23	23	21	23	20	28
Zr	85	146	131	125	136	93	135	166	82	73	69	72	60	81
Nb	4·73	8·38	6·78	7·04	6·37	4·15	9·43	9·17	3·83	4·11	3·86	4·08	3·03	4·11
Cs	0·38	1·52	1·50	1·83	2·22	1·23	0·76	1·35	1·21	1·10	0·98	1·10	0·58	0·26
Ba	492	568	635	646	545	422	446	601	419	459	407	439	265	466
La	14·7	20·3	25·7	18·7	18·2	13·6	19·6	25·2	12·1	14·9	13·7	14·4	11·6	17·0
Ce	28·6	40·7	45·2	37·8	37·8	28·4	40·3	45·9	25·3	29·9	28·3	28·9	24·2	34·3
Pr	4·01	5·42	6·14	5·23	5·15	3·96	5·41	6·89	3·55	3·98	3·75	3·89	3·42	4·93
Nd	18·0	22·7	23·8	22·8	22·3	17·4	23·5	29·5	15·8	17·6	16·4	17·1	15·1	22·0
Sm	4·44	4·94	4·49	5·50	5·24	4·29	5·28	6·37	3·86	4·18	3·81	4·06	3·54	5·20
Eu	1·47	1·54	1·26	1·77	1·50	1·30	1·63	1·73	1·19	1·37	1·26	1·34	1·18	1·66
Gd	4·97	4·90	4·00	6·01	5·48	4·47	5·52	6·54	4·23	4·30	3·98	4·21	3·80	5·33
Tb	0·81	0·76	0·58	0·96	0·85	0·71	0·85	0·98	0·66	0·66	0·61	0·64	0·57	0·80
Dy	4·75	4·43	3·28	5·68	4·99	4·12	4·98	5·72	3·85	3·87	3·60	3·77	3·36	4·67
Ho	0·99	0·92	0·66	1·18	1·02	0·85	1·04	1·21	0·79	0·81	0·74	0·79	0·70	0·95
Er	2·67	2·47	1·77	3·25	2·72	2·24	2·84	3·35	2·10	2·20	1·99	2·12	1·88	2·51
Tm	0·44	0·43	0·31	0·55	0·46	0·36	0·48	0·58	0·35	0·35	0·34	0·35	0·31	0·41
Yb	2·66	2·61	1·90	3·27	2·76	2·17	2·84	3·53	2·06	2·16	1·98	2·11	1·90	2·46
Lu	0·44	0·43	0·32	0·54	0·46	0·35	0·47	0·61	0·33	0·37	0·33	0·35	0·31	0·40

(continued)

Table 1: Continued

	Pre-caldera			Caldera	Post-caldera Caldera-rim (CR)									
					Djampit	Djampit	Djampit	Djampit	Ringgih	Ringgih	Ringgih	Ringgih	Ringgih	Pawenen
	KI 79	KI 114	KI 182	KI 85	KI 108	KI 69	KI 137	KI 136	KI 11	KI 26A	KI 26B	KI 18	KI 176	KI 178
Hf	2·36	3·67	3·33	3·43	3·53	2·49	3·43	4·24	2·25	2·06	1·92	1·98	1·66	2·29
Ta	0·34	0·74	0·67	0·73	0·85	0·43	0·74	0·67	0·33	0·40	0·43	0·37	0·25	0·28
Pb	6·3	8·3	11·4	10·1	8·5	6·1	6·3	10·0	5·7	6·9	6·3	6·0	3·3	5·6
Th	3·38	4·87	6·19	4·50	5·64	3·68	4·25	6·00	3·09	3·17	2·83	3·10	2·02	3·41
U	0·63	1·15	1·67	1·11	1·52	1·07	1·00	1·45	0·86	0·78	0·71	0·72	0·46	0·55
$^{87}Sr/^{86}Sr$	0·704252 ± 9	0·704257 ± 13	0·704188 ± 6	0·704275 ± 8		0·704219 ± 6	0·704292 ± 8	0·704272 ± 8			0·704353 ± 11		0·704231 ± 10	0·704518 ± 9
$^{143}Nd/^{144}Nd$	0·512890 ± 6	0·512891 ± 11	0·512893 ± 10	0·512875 ± 7	0·512839 ± 5	0·512859 ± 5	0·512842 ± 8	0·512850 ± 10	0·512848 ± 5		0·512827 ± 7		0·512839 ± 14	0·512785 ± 9
$^{176}Hf/^{177}Hf$	0·283113 ± 5	0·283075 ± 6	0·283097 ± 16	0·283114 ± 4	0·283121 ± 6	0·283102 ± 10	0·283063 ± 6	0·283079 ± 5	0·283103 ± 8		0·283128 ± 7		0·283064 ± 6	0·283109 ± 6

	Post-caldera																
	Caldera-rim (CR)											Kawah Ijen					
	Suket	Suket	Suket	Suket	Rante	Rante	Merapi	Merapi	Merapi	Merapi	Merapi						
	KI 165	KI 164	KI 145	KI 143	KI 202	KI 63	KI 106	KI 105	KI 116	KI 52	KI 57	KI 194		KI 162	KI 190		KI 29B
Sc	18	11	34	34	17	34	27	29	27	37	26	21		18	28		21
Ti	5395	3219	6689	7373	4484	6617	5736	6174	5496	7079	6342	5257		4975	6533		5754
V	198	85	397	389	179	314	285	281	264	333	226	197		172	306		234
Cr	0·1	0·8	4·7	4·1	2·6	18·5	9·4	7·6	12·2	8·6	1·9	5·8		3·3	4·9		1·0
Co	42	27	52	47	37	51	78	46	48	46	35	33		29	49		40
Ni	6·9	3·1	24·9	24·4	4·7	28·4	39·8	17·4	22·2	17·3	9·8	6·9		7·9	12·5		6·8
Cu	88	35	194	192	38	147	97	133	68	90	99	21		49	107		136
Zn	72	75	85	111	62	93	79	85	79	97	94	72		79	86		74
Ga	20	18	20	20	17	21	19	20	19	22	21	18		19	22		19
Rb	32·9	25·0	31·8	33·9	62·8	25·4	16·1	30·3	25·9	33·0	43·3	67·4		69·2	26·9		18·7
Sr	600	628	497	507	342	543	555	558	513	487	586	440		455	549		670
Y	23	23	23	24	26	22	26	24	21	25	27	28		27	22		21
Zr	100	97	84	88	168	78	92	92	92	107	138	170		176	81		61
Nb	4·44	4·26	3·94	4·09	7·90	3·76	4·60	4·43	4·25	5·70	6·22	8·13		7·96	3·90		3·54
Cs	1·28	0·77	1·21	1·24	2·88	0·99	0·62	1·23	0·65	0·86	1·60	2·84		2·39	0·56		0·59
Ba	554	438	433	446	484	365	368	403	365	378	507	614		659	339		381
La	15·3	15·4	12·4	12·7	19·4	13·6	16·0	16·3	14·4	15·7	19·5	20·6		19·8	12·6		12·2

Ce	31·1	29·9	26·0	26·8	39·9	28·0	33·8	32·7	30·5	32·5	40·0	41·8	39·7	26·4	25·2	
Pr	4·19	4·32	3·65	3·70	5·20	3·84	4·75	4·41	4·15	4·43	5·45	5·50	5·18	3·69	3·39	
Nd	18·0	18·8	16·5	16·6	21·2	16·9	20·8	19·1	17·8	19·1	23·0	22·7	21·5	16·4	15·3	
Sm	4·12	4·06	3·99	4·12	4·57	3·94	4·73	4·33	3·95	4·47	5·15	4·97	4·57	3·86	3·60	
Eu	1·30	1·28	1·22	1·29	1·14	1·27	1·37	1·33	1·21	1·37	1·51	1·29	1·24	1·25	1·26	
Gd	4·19	4·17	4·35	4·47	4·44	4·04	4·76	4·37	3·98	4·69	5·16	5·02	4·63	4·00	3·86	
Tb	0·65	0·63	0·67	0·70	0·70	0·63	0·71	0·68	0·62	0·72	0·77	0·76	0·74	0·63	0·59	
Dy	3·77	3·67	3·92	4·05	4·12	3·66	4·14	3·85	3·53	4·19	4·42	4·51	4·26	3·68	3·46	
Ho	0·77	0·77	0·80	0·83	0·86	0·75	0·85	0·80	0·72	0·87	0·90	0·95	0·89	0·74	0·72	
Er	2·12	2·09	2·16	2·26	2·42	2·00	2·32	2·14	1·98	2·34	2·44	2·61	2·49	2·03	1·96	
Tm	0·34	0·36	0·35	0·37	0·42	0·34	0·38	0·36	0·32	0·39	0·41	0·46	0·43	0·34	0·31	
Yb	2·12	2·15	2·08	2·18	2·55	2·02	2·24	2·14	1·96	2·34	2·44	2·73	2·60	2·08	1·92	
Lu	0·36	0·36	0·34	0·36	0·42	0·34	0·37	0·36	0·33	0·39	0·41	0·47	0·45	0·34	0·32	
Hf	2·64	2·52	2·26	2·42	4·41	2·11	2·44	2·47	2·43	2·79	3·61	4·44	4·56	2·18	1·71	
Ta	0·37	0·37	0·40	0·43	0·77	0·34	0·32	0·38	0·37	0·44	0·51	0·65	0·69	0·38	0·39	
Pb	7·5	7·3	5·5	6·3	10·4	6·7	5·9	6·9	6·7	7·2	9·0	9·8	10·8	5·5	5·0	
Th	3·77	2·47	3·17	3·42	7·33	2·90	2·96	3·65	3·08	3·90	4·85	7·44	7·22	3·01	2·39	
U	0·93	0·64	0·89	0·91	1·78	0·65	0·69	0·83	0·73	0·90	1·12	1·79	1·80	0·71	0·55	
$^{87}Sr/^{86}Sr$						0·704286 ± 9			0·704316 ± 12			0·704361 ± 10		0·704366 ± 8	0·704382 ± 8	
$^{143}Nd/^{144}Nd$			0·512847 ± 5		0·512839 ± 7	0·512855 ± 6	0·512821 ± 4		0·512808 ± 5			0·512824 ± 10		0·512825 ± 13	0·512825 ± 10	
$^{176}Hf/^{177}Hf$			0·283108 ± 8		0·283104 ± 5	0·283101 ± 6	0·283097 ± 8		0·283101 ± 7			0·283092 ± 6		0·283094 ± 10	0·283118 ± 7	

	Post-caldera													
	Kawah Ijen	Blau			Intra-caldera (IC)									
					Kukusan	Glaman	Glaman	Lingker	Anyar	Anyar	Gen./Pen.	Gen./Pen.	Gen./Pen.	Gen./Pen.
	KI 75	KI 31D	KI 29D	KI 28	KI 34	KI 35	KI 36	KI 139	KI 142	KI 92	KI 90	KI 39	KI 140	KI 89
Sc	20	23	18	16	21	15	21	20	22	22	22	22	21	21
Ti	5844	5796	4424	4094	6258	4274	5496	5934	6174	6485	6474	6294	6054	6114
V	187	287	182	171	197	127	201	192	204	210	162	207	197	199
Cr	0·2	3·7	7·0	6·6	2·3	4·3	3·4	2·2	1·1	1·8	0·2	2·0	1·7	1·8
Co	43	79	29	30	34	33	61	48	41	37	54	49	40	33
Ni	4·1	11·9	8·0	8·0	7·2	5·3	14·0	7·5	6·3	8·0	2·5	8·2	8·4	6·8
Cu	63	105	53	45	75	25	64	70	74	79	33	71	66	75
Zn	93	81	63	62	87	60	76	82	86	90	109	88	87	85
Ga	21	19	16	16	20	18	18	18	19	20	19	19	19	19
Rb	33·0	22·0	63·8	60·7	75·7	103·6	59·9	62·1	66·7	66·5	42·6	66·3	69·5	69·9
Sr	649	562	346	346	474	391	473	466	499	504	469	506	490	492

(continued)

Table 1: Continued

	Post-caldera													
	Kawah Ijen	Blau			Intra-caldera (IC)									
					Kukusan	Glaman	Glaman	Lingker	Anyar	Anyar	Gen./Pen.	Gen./Pen.	Gen./Pen.	Gen./Pen.
	KI 75	KI 31D	KI 29D	KI 28	KI 34	KI 35	KI 36	KI 139	KI 142	KI 92	KI 90	KI 39	KI 140	KI 89
Y	25	23	25	23	32	27	29	30	31	31	34	31	32	32
Zr	97	74	167	158	177	223	144	149	159	157	123	157	166	167
Nb	4·74	4·23	7·75	7·39	8·34	9·75	7·01	7·13	7·59	7·39	7·00	7·53	7·82	7·89
Cs	1·07	0·70	2·75	2·71	3·12	4·44	2·26	2·56	2·70	2·66	1·75	2·69	2·86	2·87
Ba	436	382	578	498	639	727	449	585	621	594	673	618	622	635
La	17·3	15·4	18·8	17·5	22·2	23·5	19·9	20·2	21·3	20·4	19·2	21·2	21·4	21·8
Ce	36·0	33·1	37·8	36·4	45·5	46·3	41·2	41·6	43·8	42·4	38·8	43·8	44·0	44·7
Pr	4·98	4·52	4·92	4·54	6·10	5·81	5·60	5·59	5·85	5·78	5·20	5·89	5·88	5·99
Nd	21·9	19·7	19·9	18·4	26·1	23·0	23·9	24·0	25·0	24·9	23·1	25·4	25·2	25·5
Sm	4·89	4·41	4·32	4·00	5·81	4·79	5·35	5·49	5·73	5·58	5·53	5·69	5·61	5·74
Eu	1·51	1·37	1·09	1·01	1·50	1·11	1·40	1·44	1·51	1·53	1·73	1·52	1·48	1·49
Gd	4·86	4·52	4·24	3·95	5·95	4·64	5·37	5·50	5·72	5·80	5·96	5·84	5·72	5·80
Tb	0·73	0·68	0·68	0·62	0·91	0·72	0·83	0·84	0·88	0·88	0·94	0·89	0·87	0·88
Dy	4·19	3·93	4·02	3·71	5·24	4·22	4·83	4·88	5·14	5·08	5·60	5·20	5·09	5·14
Ho	0·86	0·80	0·84	0·76	1·07	0·88	0·99	1·01	1·06	1·05	1·17	1·08	1·06	1·07
Er	2·29	2·10	2·35	2·15	2·96	2·46	2·70	2·80	2·92	2·87	3·22	2·97	2·91	2·94
Tm	0·39	0·35	0·40	0·37	0·51	0·43	0·45	0·45	0·47	0·49	0·55	0·49	0·49	0·49
Yb	2·29	2·02	2·46	2·31	3·05	2·74	2·70	2·73	2·92	2·88	3·28	2·96	2·93	2·99
Lu	0·39	0·33	0·41	0·38	0·50	0·45	0·44	0·46	0·48	0·48	0·55	0·48	0·48	0·50
Hf	2·64	2·06	4·31	4·15	4·61	5·87	3·71	3·86	4·12	4·09	3·41	4·05	4·29	4·31
Ta	0·55	0·39	0·70	0·68	0·71	0·91	0·73	0·71	0·69	0·63	0·77	0·81	0·75	0·64
Pb	7·6	5·7	10·7	10·3	11·2	17·1	9·3	9·6	9·8	9·8	10·2	10·2	10·5	10·6
Th	3·50	2·73	6·98	6·54	7·81	11·47	6·18	6·57	7·02	6·68	4·59	6·93	7·31	7·41
U	0·78	0·66	1·77	1·69	2·01	2·79	1·63	1·72	1·83	1·77	1·14	1·83	1·90	1·91
$^{87}Sr/^{86}Sr$		0·704310 ± 9		0·704304 ± 9	0·704257 ± 10	0·704317 ± 9	0·704227 ± 10		0·704231 ± 9		0·704221 ± 8			
$^{143}Nd/^{144}Nd$		0·512803 ± 4		0·512857 ± 6	0·512837 ± 8	0·512835 ± 10	0·512843 ± 6		0·512879 ± 9		0·512854 ± 6			
$^{176}Hf/^{177}Hf$		0·283104 ± 8		0·283097 ± 4	0·283078 ± 5	0·283095 ± 5	0·283101 ± 6		0·283099 ± 7		0·283105 ± 5			

Gen./Pen., Genteng/Pendian. Errors on isotope ratios are within-run 2SE on the final quoted significant figure. Details of isotope data accuracy and precision are given in the analytical techniques section.

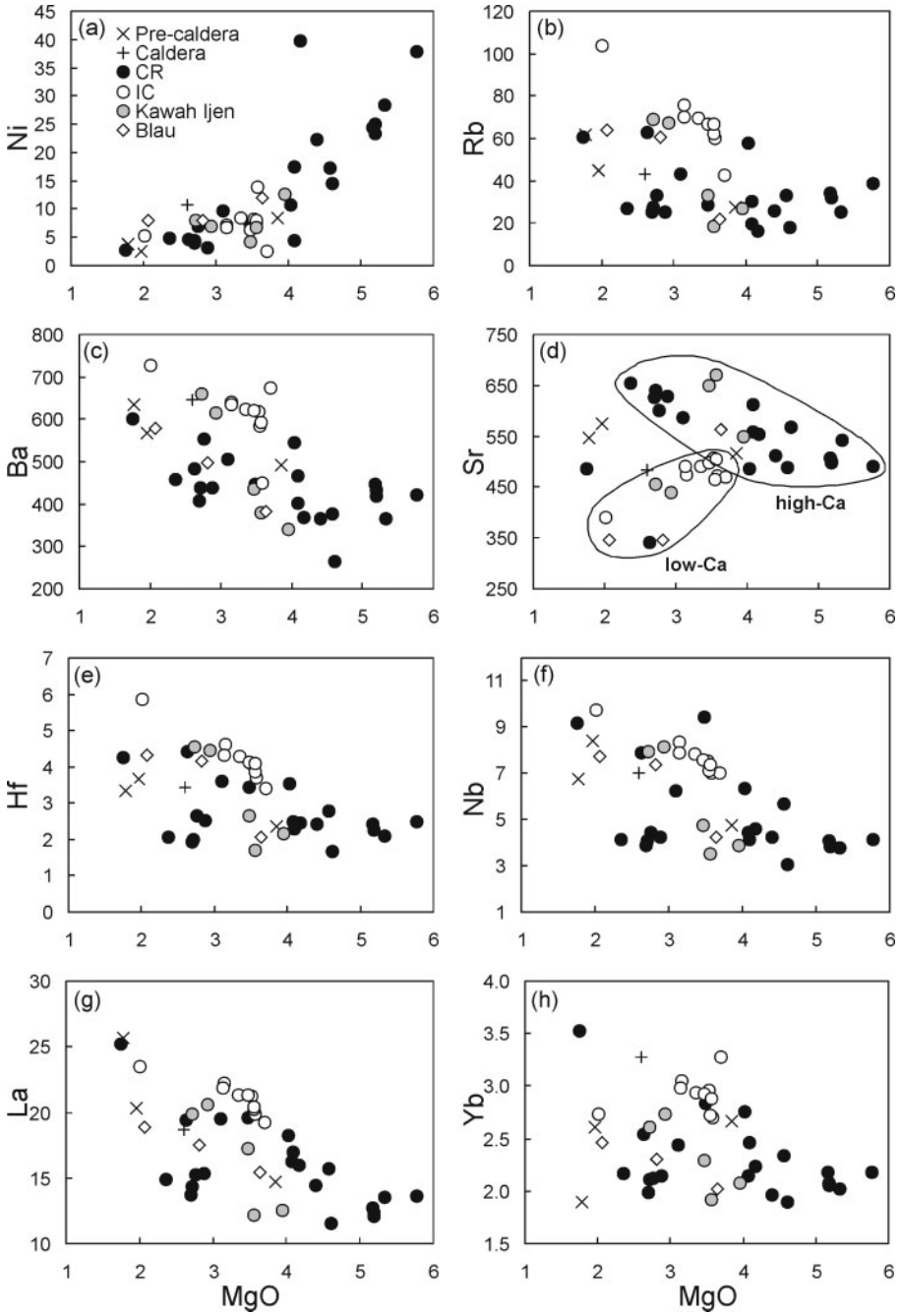

Fig. 4. Trace element variation diagrams vs wt % MgO as a differentiation index for selected trace elements in IVC volcanic rocks.

complex are among the least radiogenic Sr and most radiogenic Nd isotopic values reported for Javanese volcanoes (Fig. 6a); only samples from Guntur (Edwards, 1990) and Galunggung (Gerbe *et al.*, 1992) have higher $^{143}Nd/^{144}Nd$ and lower $^{87}Sr/^{86}Sr$ ratios. The Sr isotope ratios of the IVC lavas are consistent with the previously recognized eastward decrease in $^{87}Sr/^{86}Sr$ from West Java to Bali (Whitford, 1975). In Nd–Hf isotope space the IVC lavas lie on the edge of the Java field close to the Indian Ocean MORB field (Fig. 6b). The pre-caldera group has relatively low $^{87}Sr/^{86}Sr$ ratios (0·704169–0·704238) and are indistinguishable from one another in $^{143}Nd/^{144}Nd$ (0·512892–0·512895). However, their range in $^{176}Hf/^{177}Hf$ (0·283081–0·283118) is comparable with the range of Hf isotope ratios seen in the volcanic complex as a whole (Fig. 6b inset). IC $^{143}Nd/^{144}Nd$ values are similar to those of the CR group with no obvious division between the two groups. The IC lavas display a more limited range in $^{176}Hf/^{177}Hf$

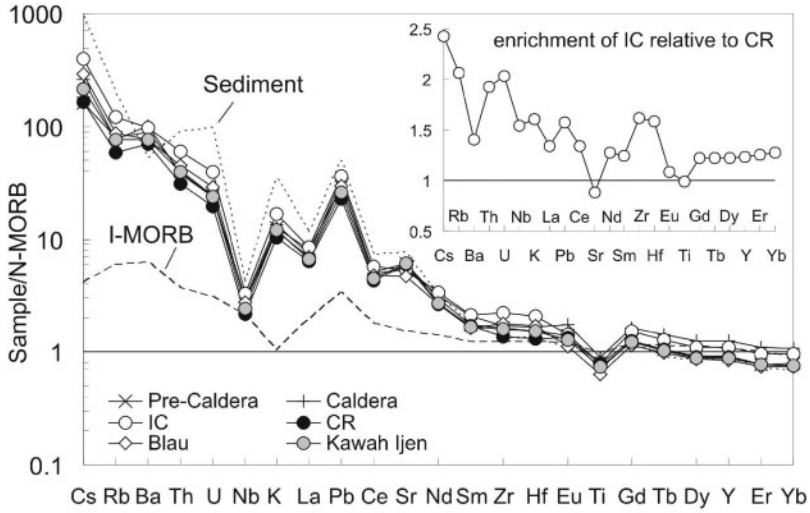

Fig. 5. N-MORB normalized trace element diagram for IVC volcanic rocks. Inset diagram shows the average enrichment of the IC group relative to the CR group. Averages calculated using CR and IC rock samples of similar MgO content (between 3 and 4 wt % MgO). Data sources: Indian Ocean MORB (I-MORB): Chauvel & Blichert-Toft (2001); N-MORB normalization values: Sun & McDonough (1989); Sediment: Vroon *et al.* (1995) (Track III).

ratios, but plot in the centre of the larger spread of the CR group (Fig. 6b inset).

Oxygen isotope data

The $\delta^{18}O$ values of clinopyroxene, olivine and plagioclase are +5·38 to +5·58‰ ($n=5$), +5·02‰ ($n=1$) and +6·08‰ ($n=1$), respectively (Table 2). The range of clinopyroxene $\delta^{18}O$ values is narrow and comparable with the average mantle $\delta^{18}O$ value of $+5{\cdot}57 \pm 0{\cdot}32$‰ (Ionov *et al.*, 1994; Mattey *et al.*, 1994). IVC $\delta^{18}O$ clinopyroxene values are lower than those of plagioclase and higher than those of olivine; with coexisting mineral pair Δ_{cpx-ol} and $\Delta_{plag-cpx}$ values of 0·36‰ and 0·5‰, respectively, suggesting isotopic equilibrium at typical magmatic temperatures for andesite liquids (Macpherson & Mattey, 1998; Macpherson *et al.*, 1998). The limited dataset displays no noticeable difference in the cpx $\delta^{18}O$ values of the different geographical groups.

The oxygen isotope ratios of clinopyroxene phenocrysts from IVC rocks are within the range reported for clinopyroxene from the primitive Galunggung lavas from West Java (+5·3 to +5·6‰, Harmon & Gerbe, 1992), and clinopyroxene and olivine $\delta^{18}O$ values lie at the lower end of the Banda arc $\delta^{18}O$ range (+5·18 to +7·04‰ and +4·92 to +5·59‰, respectively; Vroon *et al.*, 2001). The $\delta^{18}O$ value for the only plagioclase sample analysed from the IVC is within error of the $\delta^{18}O$ range of Galunggung lavas (+5·6 to +6·0‰; Harmon & Gerbe, 1992) and is lower than $\delta^{18}O$ values recorded in plagioclase phenocrysts from Merapi volcanic rocks (+6·5 to +7·00‰, Gertisser & Keller, 2003). The $\delta^{18}O$ values of the IVC rocks also are close to the values postulated for the upper mantle in other subduction zones (Smith *et al.*, 1996; Thirlwall *et al.*, 1996; Macpherson & Mattey, 1998; Macpherson *et al.*, 1998, 2000; Eiler *et al.*, 2000).

DISCUSSION

Magmatic differentiation processes

Differentiation processes can significantly change the composition of magmas as they rise through the lithosphere towards the surface. It is important to identify the impact of these processes on the composition of the magma to remove uncertainty in establishing the composition and magnitude of slab-derived contributions to the mantle source in subduction zones. Low MgO, Ni and Cr abundances in IVC volcanic rocks indicate that they are not primary mantle melts, and that magma compositions were, therefore, modified *en route* to the Earth's surface.

Correlations of various major and trace elements with indices of differentiation (i.e. MgO) in IVC lavas (Figs 3 and 4) suggest that the concentrations of some elements are controlled by shallow-level differentiation processes such as fractional crystallization, magma mixing or contamination. Major and trace element variations for most of the post-caldera samples can be described as one of two trends, which are exemplified in the CaO vs MgO diagram (Fig. 3d), where a low-Ca group, dominantly consisting of the IC samples, displays a positive correlation, and a high-Ca group, composed of most CR samples along with some Kawah Ijen and Blau samples, shows little change in CaO with decreasing MgO. Similar trends are apparent in plots of Al_2O_3 and Sr against MgO (Figs 3b and 4d). Higher modal plagioclase abundances

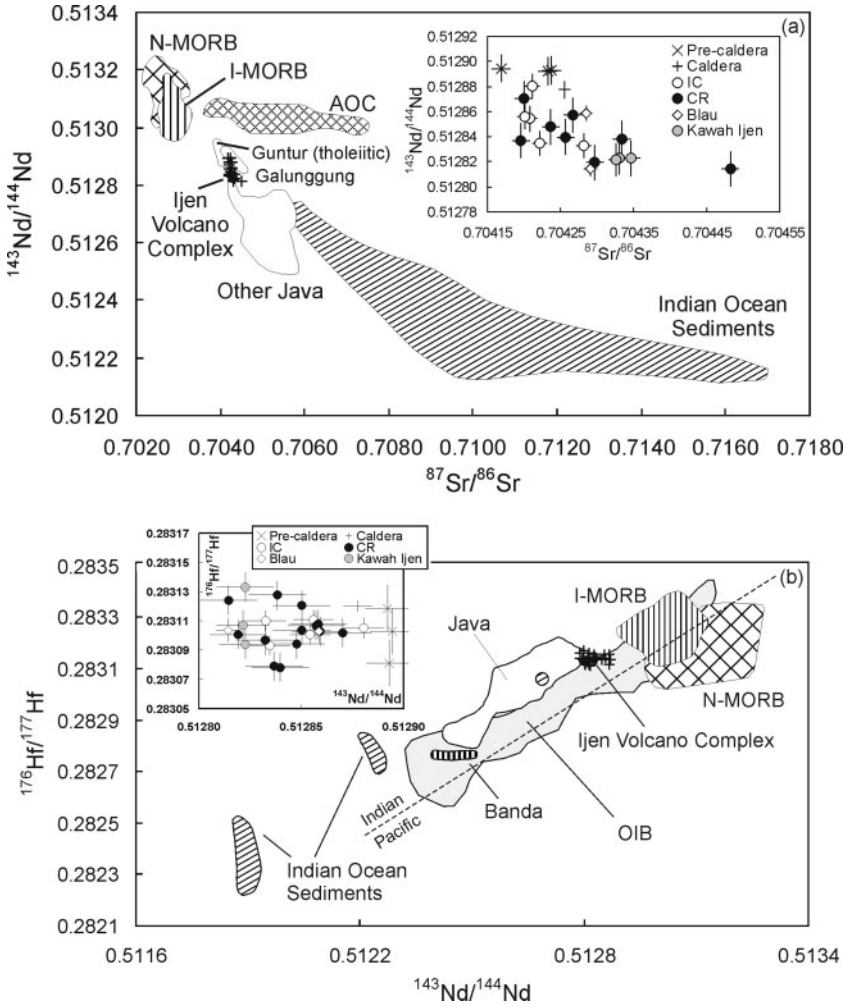

Fig. 6. (a) Variation of $^{143}Nd/^{144}Nd$ vs $^{87}Sr/^{86}Sr$ for the IVC. Inset: Nd and Sr isotope diagram for the IVC groups. The lack of any distinction in isotope ratio between the IC and CR groups should be noted. Data sources: I-MORB: Price *et al.* (1986), Ito *et al.* (1987), Rehkämper & Hofmann (1997) and Chauvel & Blichert-Toft (2001); N-MORB: Ito *et al.* (1987) and Chauvel & Blichert-Toft (2001); altered oceanic crust (AOC): Staudigel *et al.* (1995); other Java volcanic rocks: Whitford *et al.* (1981), White & Patchett (1984), Edwards (1990, including Guntur tholeiites), Gerbe *et al.* (1992, Galunggung) and Gertisser & Keller (2003); Indian ocean sediments: Ben Othman *et al.* (1989) and Gasparon & Varne (1998). (b) Variation of $^{176}Hf/^{177}Hf$ vs $^{143}Nd/^{144}Nd$ for the IVC. Inset: Hf–Nd isotope diagram of IVC volcanic rocks separated by eruptive group. Data sources: I-MORB: Salters (1996), Nowell *et al.* (1998) and Chauvel & Blichert-Toft (2001); N-MORB: I-MORB references listed for (a) plus Salters & Hart (1991); OIB: Patchett & Tatsumoto (1980), Patchett (1983), Stille *et al.* (1986), Salters & Hart (1991), Nowell *et al.* (1998) and Salters & White (1998); Java: White & Patchett (1984) and Woodhead *et al.* (2001); Banda: White & Patchett (1984); Indian ocean sediments: White *et al.* (1986), Ben Othman *et al.* (1989) and Vervoort *et al.* (1999). Dividing line for Indian and Pacific MORB provenance from Pearce *et al.* (1999). Maximum 2σ external errors for each geographical group are shown in the inset diagrams.

(~10%, Table 3), and a less pronounced negative Eu anomaly in high-Ca lavas (Fig. 7) suggest that the different geochemical trends exhibited by the low-Ca and high-Ca groups may be due to more extensive plagioclase fractionation in the former, or plagioclase accumulation in the latter. Possible evidence for open-system processes in the petroenesis of the IVC lavas includes: coexistence of phenocrysts (plagioclase and clinopyroxene) that display normal, oscillatory and reverse zoning (Sitorus, 1990); clinopyroxene overgrowths on orthopyroxene phenocrysts; and bimodal distributions in plagioclase core compositions (Sitorus, 1990, see Electronic Appendix 2; Berlo 2001). One group of plagioclase crystal cores cluster below An_{60}, and the other generally above An_{80}. However, bimodal plagioclase compositions are found within volcanic rocks from both the high- and low-Ca groups, indicating that although mixing may occur, it is not the dominant control on chemical variation, otherwise we would only expect to find bimodal plagioclase populations in high-Ca rocks. Also, higher modal plagioclase abundance (Table 3; Electronic Appendix 3) does not necessarily indicate accumulation; it may just be a result of a greater degree of crystallization or more plagioclase in the modal equilibrium assemblage. Variations in the fractionating mineral

Table 2: Oxygen isotope compositions of IVC post-caldera volcanic rocks

	Caldera-rim (CR)	Intra-caldera (IC)			Blau
	Rante	Kukusan	Glaman	Glaman	
Sample:	KI 63	KI 34	KI 35	KI 36	KI 31D
δ^{18}O cpx	+5·38	+5·51	+5·49	+5·58	+5·46
δ^{18}O ol	+5·02				
δ^{18}O plag				+6·08	

O isotope data reported as per mil (‰). cpx, clinopyroxene; ol, olivine; plag, plagioclase.

assemblage can produce contrasting differentiation trends on variation diagrams (e.g. Davidson, 1996). Crystallization vectors drawn in Fig. 3b and d illustrate the magmatic evolution predicted for primitive IVC magma during fractionation of different mineral assemblages. The different trends observed in the high- and low-Ca groups can result from differences in the phases that make up the fractionating assemblage and their proportions. Assemblages consisting of clinopyroxene and olivine ± plagioclase can replicate the high-Ca array (Fig. 3b and d), whereas the same assemblage but with more plagioclase fractionation relative to clinopyroxene and olivine is suggested for the low-Ca trend (see labelled arrows, Fig. 3b and d). Less plagioclase fractionation in the evolution of the high-Ca lavas, relative to the low-Ca lavas, is also consistent with the variations of Al_2O_3, Sr and Ba with respect to MgO, along with a smaller negative Eu anomaly.

Fractional crystallization

The XLFRAC, least-squares major element modelling technique (see Stormer & Nicholls, 1978) was used to ascertain whether the high-Ca and low-Ca differentiation trends can be explained by differences in the amount of plagioclase fractionation, and also to determine whether compositional variation within and between geographical groups (e.g. IC, CR, Kawah Ijen) can be explained by fractional crystallization. Models 1 and 2 in Table 3 suggest that the most evolved post-caldera rocks of the high-Ca and low-Ca groups can be produced by fractionation of plagioclase, clinopyroxene, olivine and Fe–Ti oxide from the least evolved samples of their respective groups ($\sum r^2 = 0{\cdot}2$ and 0·19, respectively). Models of fractionation to other high-Ca and low-Ca group daughter compositions (models 3–6 and 7–9, respectively) yield excellent $\sum r^2$ values (<0·16). All of these models also suggest that significantly less plagioclase fractionation is required from the parent magma to reach high-Ca daughter compositions (10–12%) compared with those with low-Ca (~20–37%). Therefore, we suggest that the different (high- and low-Ca) trends (e.g. Fig. 3b and d) are due to a greater amount of plagioclase fractionation in the IC rocks than in the CR rocks.

Least-squares analysis demonstrates that intra-group CR fractionation models yield low $\sum r^2$ values (models 2–9, Table 3). A good solution ($\sum r^2 = 0{\cdot}02$) is also obtained for a model using a less evolved IC sample as parent to a more evolved IC rock (model 10). Low $\sum r^2$ values are obtained in model 11, between the two Kawah Ijen samples, which straddle the high-Ca and low-Ca trends on several major element diagrams. Some inter-group models can also generate very acceptable results (models 13–15), suggesting that members of the different geographical groups can be related to each other through fractional crystallization. However, least-squares modelling cannot generate low $\sum r^2$ in models where IC rocks represent the parent magma composition and CR is the daughter, unless crystals are accumulated rather than removed (models 16 and 17).

Utilizing the phase proportions and degree of crystallization predicted from the major element modelling (Table 3) it is possible to test the conclusions of least-squares analysis by modelling trace element concentrations using the Rayleigh fractionation equation $C_l = C_o F^{(D-1)}$, where C_l and C_o represent the concentration of an element in the daughter and parental liquids, respectively, F is the fraction of liquid remaining and D is the bulk distribution coefficient. The distribution coefficients used in modelling are given in Table 4. The results of selected trace element models are given in Table 5 and show excellent agreement between calculated and observed daughter concentrations. The strongest agreement (model 10) is between the intra-caldera samples KI 92 and KI 34 in the low-Ca group, where calculated values lie within 10% of the measured concentrations. In summary, trace element modelling validates models of fractional crystallization developed from major element data; this suggests that fractional crystallization is the main control on melt evolution at IVC. It also confirms that the separate trends of the low-Ca and high-Ca groups are likely to be due to variable influence of plagioclase in the fractionating mineral assemblage and are not a result of plagioclase accumulation in the high-Ca group.

Structural controls on magma ascent and storage

The location of the CR volcanoes around the caldera rim suggests that ring fractures may facilitate the movement of magma below these volcanoes. This has been proposed for other post-caldera vents located along radial fractures within volcanic complexes, such as Roccamonfina volcano in Italy (Giannetti, 2001) and Chichontepec volcanic centre in El Salvador (Rotolo & Castorina, 1998). The linear orientation (roughly NE–SW, Berlo, 2001) of

Table 3: Results of major element least-squares modelling

Model no.			Initial (parent)	Geog. group	Final (daughter)	Geog. group	ΔMgO (wt %)	$\sum r^2$	% removed				%	D thin-section abundance			
									Plag	Cpx	Ol	Fe–Ti	Cryst.	Plag%	Cpx%	Ol%	Fe–Ti%
1	most to least evolved	low-Ca	KI 63	CR	KI 35	IC	3·32	0·20	45·2	12·1	7·9	6·2	71	23	6	–	5
2	most to least evolved	high-Ca	KI 11	CR	KI 26A	CR	2·83	0·19	11·8	4·9	8·9	2·6	28	36	7	1	6
3	high-Ca group daughter		KI 145	CR	KI 57	CR	2·09	0·07	12·4	7·8	3·3	5·8	29	37	4	1	3
4			KI 63	CR	KI 18	CR	2·62	0·10	11·4	4·3	7·2	1·4	24	34	6	1	4
5			KI 63	CR	KI 26B	CR	2·63	0·09	10·1	3·7	7·5	1·5	23	33	7	1	5
6			KI 52	CR	KI 57	CR	1·47	0·16	–	6·4	2·7	1·1	10	37	4	1	3
7	low-Ca group daughter		KI 63	CR	KI 202	CR	2·7	0·10	37·3	9·0	5·1	7·8	59	25	9	–	7
8			KI 145	CR	KI 108	CR	1·16	0·07	21·8	6·2	2·5	5·2	36	23	6	1	4
9			KI 11	CR	KI 108	CR	1·16	0·02	20·4	5·9	2·5	5·5	34	23	6	1	4
10	within geog. groups		KI 92	IC	KI 34	IC	0·41	0·02	10·3	1·5	2·0	1·3	15	16	6	–	6
11			KI 190	K. IJEN	KI 194	K. IJEN	1·02	0·04	39·6	6·9	4·8	4·4	56	31	9	–	3
12			KI 31D	BLAU	KI 28	BLAU	0·82	0·23	50·6	5·1	7·2	4·1	67	25	10	1	4
13	between geog. groups		KI 31D	BLAU	KI 92	IC	0·08	0·07	39·3	4·2	5·0	2·5	51	28	8	–	5
14			KI 190	K. IJEN	KI 57	CR	0·85	0·05	15·6	5·9	2·3	2·1	26	37	4	1	3
15			KI 63	CR	KI 162	K. IJEN	2·61	0·13	39·9	10·8	7·3	5·5	63	28	11	–	4
16			KI 92	IC	KI 18	CR	0·85	0·07	**36·7**	**12·0**	4·8	**4·9**	58	34	6	1	4
17			KI 92	IC	KI 136	CR	1·81	1·46	27·8	4·8	5·9	3·9	42	39	9	–	4

XLFRAC least-squares modelling based on nine oxides. Mineral compositions taken from phenocrysts in the basic and intermediate IVC rocks (see Electronic Appendix 2 for representative mineral data). The mineral phases considered in modelling are limited to those observed as phenocrysts in either the parent or the daughter rocks (Electronic Appendix 3). ΔMgO wt %, difference calculated between parent and daughter compositions; Plag, plagioclase; Cpx, clinopyroxene; Ol, olivine; Fe–Ti, Fe–Ti oxide; D, daughter; % removed is relative to initial parent magma. Phase percentages in bold indicate addition rather than removal of that phase.

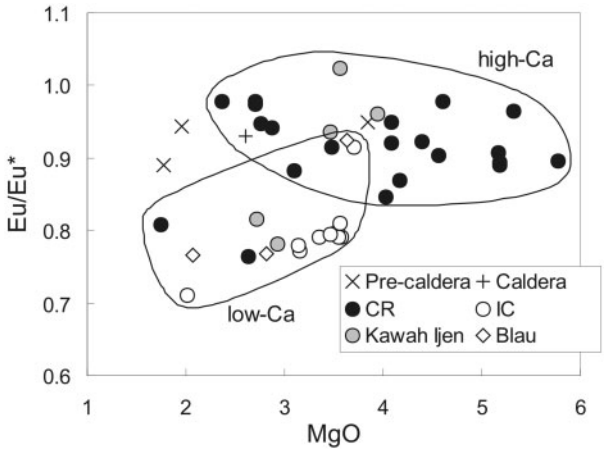

Fig. 7. Europium anomaly (Eu/Eu*) vs MgO for IVC rocks.

Table 4: Distribution coeffiecients used in trace element modelling

	ol	cpx	plag	mag
Rb	0·021	0·033	0·113	0·150
Ba	0·044	0·038	0·440	0·183
Th	0·26	0·035	0·059	0·235
U	0·083	0·016	0·112	0·11
Nb	0·027	0·168	0·275	0·837
Ta	0·059	0·123	0·057	1·113
Sr	0·048	0·139	2·512	0·11
Zr	0·03	0·197	0·098	0·727
Hf	0·37	0·297	0·031	0·353

Distribution coefficients calculated as average values for basaltic–andesitic–dacitic systems taken from the GERM database (http://earthref.org/GERM/index.html). OL, olivine; CPX, clinopyroxene; PLAG, plagioclase; mag, magnetite.

the intra-caldera volcanoes also suggests that magma below the central part of the caldera is utilizing lines of weakness and further highlights the structural control on the location of post-caldera volcanoes at IVC.

The different fractionation trends exhibited by the low-Ca (dominantly the intra-caldera rocks) and high-Ca (dominantly the caldera-rim rocks) suggest that spatial variations in chemistry within the volcanic complex might be linked to sub-volcanic structure. The contrast in geochemistry is proposed to result from differences in the amount of plagioclase fractionation from the respective magmas. Experimental evidence (Grove *et al*., 2003) suggests that plagioclase crystallization is suppressed by high water contents and high pressure in basaltic andesite magmas. Therefore, the more extensive plagioclase fractionation inferred for the IC group magmas could result from either shallower level (i.e. lower pressure) storage or lower water contents (or both) in the IC magmas relative to the CR magmas. The volatile content of magmas is also controlled by pressure; thus, the suppression of plagioclase crystallization in the CR group could be a result of magmatic differentiation at deeper levels in the crust below the caldera-rim volcanoes (Fig. 8). Magmas stored at greater depth, with higher volatile contents, might be expected to erupt more explosively than those stored at shallower levels, from which eruptions might be more passive. The presence of large stratovolcanoes on the caldera-rim and dominantly small cinder cones inside the caldera at IVC is consistent with the type of eruption, compatible with this interpretation. Therefore, at IVC it is proposed that volcanic structure exerts some control on the depths at which the rising magma can pond. Kawah Ijen erupts lavas belonging to both the low-Ca and high-Ca trends. Kawah Ijen lies at the intersection between the caldera rim and the northeastern edge of the intra-caldera lineation (Fig. 2) and could, therefore, tap both shallow and deeply ponded magmas (Fig. 8). There is no temporal division in the production of high-Ca and low-Ca lava types at Kawah Ijen, and no evidence for physical mingling or mixing (Berlo, 2001), implying separate magmatic pathways for magmas erupted from different depths (Fig. 8).

Role of crustal contamination

There is considerable evidence from other island arcs (Thirlwall & Graham, 1984; Davidson *et al*. 1987; Ellam & Harmon, 1990; Davidson, 1996; Smith *et al*., 1996; Thirlwall *et al*., 1996; Macpherson *et al*., 1998) for the contamination of primary magmas by the arc crust. Contamination is also believed to be an important process, responsible for modifying isotope ratios, in the western Sunda arc (Gasparon *et al*., 1994; Gasparon & Varne, 1998) and at Sangeang Api volcano in the East Sunda arc (Turner *et al*., 2003). Therefore, prior to discussing magma source compositions it is important to assess the role of crustal contamination at IVC. The absence of correlations between IVC Sr, Nd and Hf isotope ratios and indices of differentiation (e.g. MgO, Fig. 9) and the restricted ranges of Sr, Nd and Hf isotope ratios in IVC samples (Table 1) are consistent with a negligible input of isotopically distinct crust during differentiation. Clinopyroxene $\delta^{18}O$ values in the IVC lavas are homogeneous (+5·38 to +5·58‰, Table 2) and low, lying within the range of mantle $\delta^{18}O$ values (+5·57 ± 0·32‰) reported by Mattey *et al*. (1994) and Ionov *et al*. (1994). Therefore, it is unlikely that the lavas have been contaminated by upper crustal materials, which typically possess high $\delta^{18}O$ values, such as those reported by Gertisser & Keller (2003) for the local upper crust (calcareous sediments) in Central Java (+20·5‰ and +18·9‰).

Table 5: Results of trace element fractional crystallization modelling

Model no.:	3	6	7	8	10	11
Parent:	KI 145	KI 52	KI 63	KI 145	KI 92	KI 190
Daughter:	KI 57	KI 57	KI 202	KI 108	KI 34	KI 194
Centres:	CR–CR	CR–CR	CR–CR	CR–CR	IC–IC	K.Ijen–K.Ijen
To group:	high-Ca	high-Ca	low-Ca	low-Ca	low-Ca	high–low Ca
$\sum r^2$	0·07	0·16	0·10	0·07	0·02	0·04
PLAG	12·41	–	37·32	21·81	10·3	39·61
CPX	7·82	6·35	8·99	6·16	1·53	6·94
OL	3·32	2·7	5·14	2·46	2	4·84
Fe–Ti	5·75	1·05	7·79	5·18	1·32	4·43
Total	29·30	10·1	59·24	35·61	15·15	55·82
F	0·71	0·90	0·41	0·64	0·85	0·44
Calculated						
Rb	43·7	36·6	57·1	47·4	77·2	56·3
Ba	564	417	677	587	663	584
Th	4·32	4·28	6·54	4·73	7·75	6·34
U	1·22	0·99	1·45	1·32	2·05	1·48
Nb	4·97	6·21	6·98	5·31	8·32	7·00
Ta	0·51	0·48	0·70	0·56	0·72	0·76
Sr	476	536	311	385	447	283
Zr	110	117	161	120	181	162
Hf	2·98	3·00	4·55	3·30	4·72	4·48
Measured						
Rb	43·3	43·3	62·8	57·7	75·7	67·4
Ba	507	507	484	545	639	614
Th	4·85	4·85	7·33	5·64	7·81	7·44
U	1·12	1·12	1·78	1·52	2·01	1·79
Nb	6·22	6·22	7·90	6·37	8·34	8·13
Ta	0·51	0·51	0·77	0·85	0·71	0·65
Sr	586	586	342	487	474	440
Zr	138	138	168	136	177	170
Hf	3·61	3·61	4·41	3·53	4·61	4·44

$\sum r^2$ values, phase proportions (%) and model number taken from Table 3. Trace element concentrations in ppm.

Furthermore, only igneous cumulate xenoliths have been found within the Ijen complex lavas; continental-type crustal xenoliths have not been detected (Sitorus, 1990; Berlo, 2001). Monomineralic plagioclase xenoliths are present in lavas erupted from Anyar (IC) and Blau, and cumulate xenoliths containing plagioclase, olivine, clinopyroxene and Ti-magnetite have been found in Rante (CR) and Kawah Ijen lavas. A cumulate containing olivine, ortho- and clinopyroxene was also found in lava from Kukusan (Berlo, 2001).

Similar to conclusions reached in studies of other Sunda arc volcanoes (Gerbe *et al.*, 1992; Elburg *et al.*, 2002; Gertisser & Keller, 2003), the evidence above suggests that any interaction of IVC magmas with the arc crust during differentiation has had a negligible impact on their geochemistry. Fractional crystallization, therefore, appears to be the dominant differentiation process controlling geochemical variations in IVC lavas. Higher Sr and lower Nd and Hf isotope ratios in IVC rocks relative to MORB point towards contamination of the IVC source by an isotopically distinct crustal component.

Magma source components

Most models of magma petrogenesis at island arcs involve three main source components: (1) the mantle wedge;

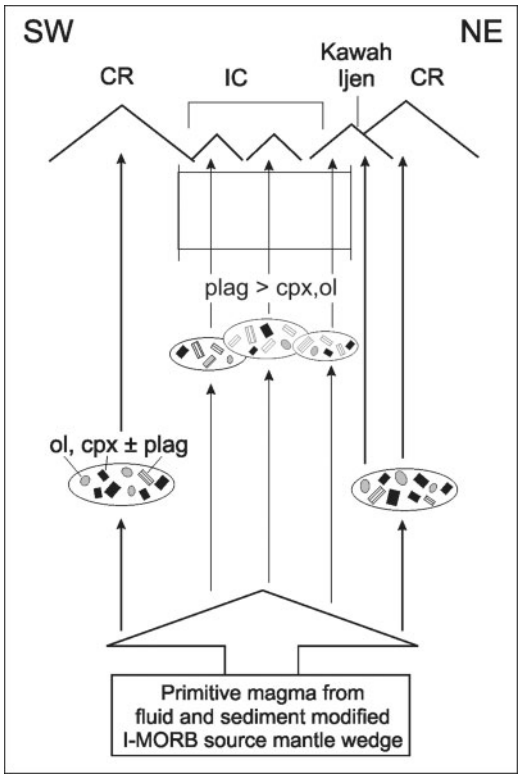

Fig. 8. Simplified diagram of magma petrogenesis at IVC, focusing on crustal level differentiation. Cross-section shown is oriented roughly parallel to the lineation of the intra-caldera volcanoes. The diagram shows the envisaged deeper level storage of magma below the CR volcanoes, and shallower level storage plus more extensive plagioclase fractionation below the IC volcanoes. Kawah Ijen is thought to tap both the shallow and deep reservoirs and transport the magma through unconnected pathways. It should be noted that Fe–Ti oxide is also fractionating in both the shallow and deep reservoirs.

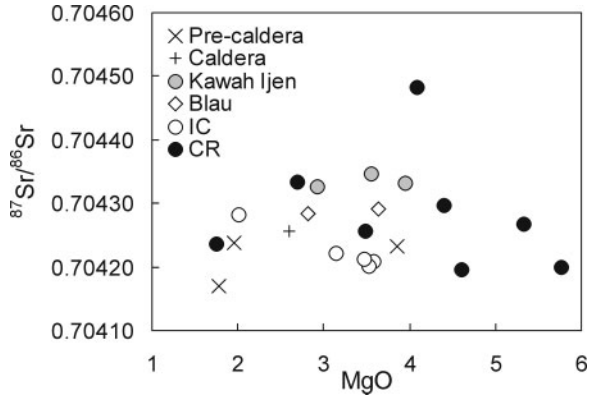

Fig. 9. $^{87}Sr/^{86}Sr$ vs MgO for IVC groups. The 2σ external errors are less than data symbol size.

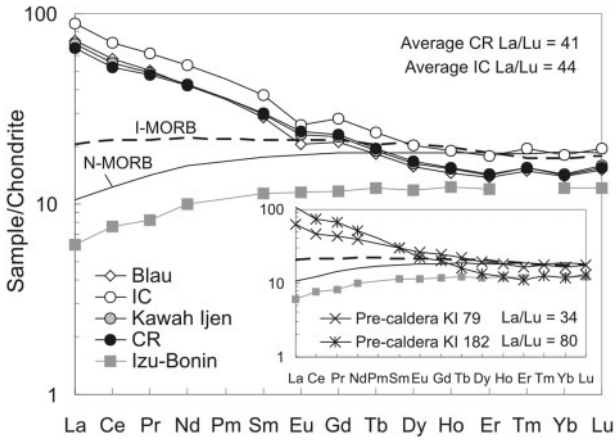

Fig. 10. Chondrite-normalized rare earth element variation in post-caldera IVC volcanic rocks. Normalizing factors and N-MORB values from Sun & McDonough (1989). Indian MORB (Chauvel & Blichert-Toft, 2001), and Izu–Bonin arc lava compositions (Taylor & Nesbitt, 1998) are shown for comparison. Inset shows the chondrite-normalized abundance of the pre-caldera volcanic rocks. The large difference in La/Lu ratios displayed by the pre-caldera group (inset) in comparison with the IC and CR groups should be noted.

(2) the subducting slab (oceanic crust and associated sediments); (3) the arc lithosphere. The majority of island arc magmas are thought to originate in the mantle wedge (Ringwood, 1974; Ellam & Hawkesworth, 1988; McCulloch & Gamble, 1991), which has been inferred by several workers to be similar to the source of MORB (Davidson, 1987; Woodhead *et al.*, 1993; Gamble *et al.*, 1996; Turner *et al.*, 2003). It has been proposed that there might be contribution from an enriched mantle component [ocean island basalt (OIB) source] in some Sunda arc lavas (Wheller *et al.*, 1987; Edwards *et al.*, 1991, 1993; van Bergen *et al.*, 1992), although a MORB-source-like mantle source has been advocated for the Sunda arc by others (e.g. White & Patchett, 1984; Turner & Foden, 2001; Elburg *et al.*, 2002). Helium isotope values of olivine crystals in mantle xenoliths and island arc volcanic rocks also implicate a MORB-source-like mantle source in the western Sunda arc (Hilton & Craig, 1989; Gasparon *et al.*, 1994).

Mantle source characteristics

The HREE and HFSE are thought to remain relatively immobile compared with other elements, such as LILE, during slab dehydration (Tatsumi *et al.*, 1986; Kessel *et al.*, 2005) and abundances are generally too low in oceanic and continental crust (Taylor & McLennan, 1985) to significantly alter ratios of these elements in magmas derived from the mantle. We can use these trace elements, therefore, to help ascertain the pre-subduction composition of the mantle wedge. HREE concentrations are ~10–15 times chondrite values in IVC lavas and display relatively flat profiles (Fig. 10). This suggests that garnet is not an important residual mineral in the source region and that the IVC magmas are derived largely from a shallow mantle source, above the garnet–spinel transition for wet peridotite. The La/Lu ratios of CR (41) and IC (44) lavas

Table 6: Average trace element ratios in I-MORB, N-MORB, bulk Java sediment and the range in IVC rocks

Ratio	I-MORB	N-MORB	Bulk Java sediment	IVC
Ta/Nb	0·07	0·06	0·08	0·07–0·13
Zr/Nb	26	32	13	14–23
Ce/Pb	15	25	3	3–7
Th/Yb	0·17	0·04	3	1–4
Ba/La	7	3	27	23–36
Sr/Nd	14	12	6	16–44

Data sources: I-MORB: Chauvel & Blichert-Toft (2001), $n=8$; N-MORB: Sun & McDonough (1989); bulk Java sediment: Plank & Langmuir (1998).

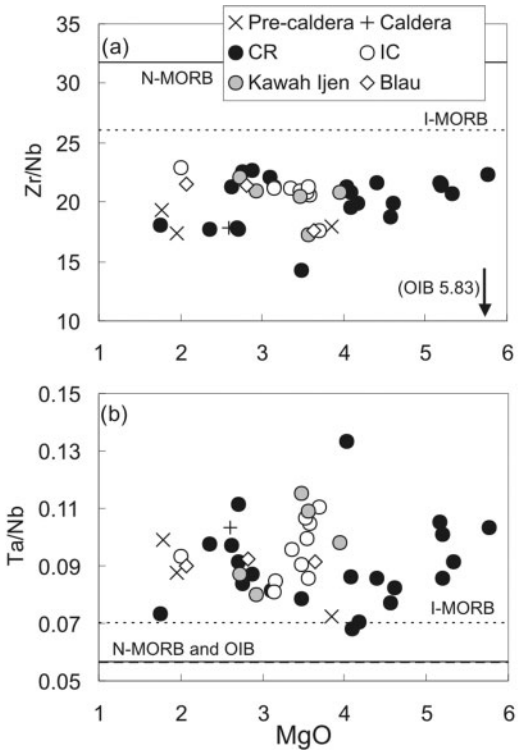

Fig. 11. (a) Zr/Nb and (b) Ta/Nb vs MgO (wt %) for IVC groups. N-MORB and OIB data from Sun & McDonough (1989). Indian MORB data from Chauvel & Blichert-Toft (2001).

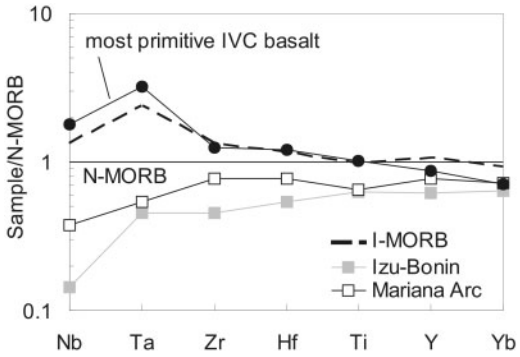

Fig. 12. Comparison of HFSE, Y and Yb abundances in the most primitive IVC basalt with N-MORB (Sun & McDonough, 1989), I-MORB (Price *et al.*, 1986; Rehkämper & Hofmann, 1997; Chauvel & Blichert-Toft, 2001) and other island arc lavas: Izu–Bonin (Taylor & Nesbitt, 1998) and Marianas arc (Elliott *et al.*, 1997).

are very similar, which is consistent with a similar source mineralogy and degree of partial melting for these two post-caldera groups. The large difference in La/Lu ratios within the three pre-caldera group samples (34–80), when compared with the fairly constant ratio of the post-caldera volcanics (~42) might be due to variable degrees of partial melting and/or different source mineralogies for the pre-caldera rocks. If post-caldera rocks from the IC and CR volcanoes, Kawah Ijen and Blau share the same source then they should possess similar ratios of immobile trace elements generally assumed to be unmodified by subduction processes (Table 6). Zr/Nb [17–23 (except one CR sample at 14)] and Ta/Nb (0·07–0·13) ratios do not change significantly with differentiation (Fig. 11a and b) and are relatively homogeneous in all IVC eruptive rocks. Zr/Nb ratios are similar to those of MORB [normal and Indian type (N-MORB and I-MORB)] whereas Ta/Nb ratios are comparable with both MORB and OIB (Table 6; e.g. Fig. 11). The similarity between HFSE and HREE concentrations in primitive IVC basalts and I-MORB, rather than N-MORB, is also apparent in Fig. 12. Therefore, we suggest that the mantle wedge beneath the IVC is similar to the source of I-MORB. Several studies utilizing Pb isotopic and trace element data have reached a similar conclusion for magmatism in SE Asia throughout the Cenozoic (Taylor *et al.*, 1994; Hickey-Vargas, 1998; Macpherson & Hall, 2001, 2002; Elburg *et al.*, 2002; Macpherson *et al.*, 2003). The HFSE and HREE concentrations and ratios of IVC lavas also indicate that the mantle wedge is not significantly depleted beneath East Java, in contrast to others arcs such as Izu–Bonin and Mariana (Fig. 12), where mantle sources are thought to have experienced melt extraction prior to their involvement in arc petrogenesis (Woodhead *et al.*, 1993; Elliott *et al.*, 1997; Taylor & Nesbitt, 1998).

Sr is fluid-mobile during slab dehydration, therefore, Sr isotope data are not well suited for identifying the isotopic composition of the precursor mantle wedge. Experimental work (Tatsumi *et al.*, 1986; Brenan *et al.*, 1995; You *et al.*, 1996) and studies of arc lavas (McCulloch & Gamble, 1991; Pearce & Peate, 1995; Münker *et al.*, 2004) indicate that Hf and Nd are relatively immobile during slab dehydration, particularly with respect to the formation of aqueous fluids (Kessel *et al.*, 2005). However, Woodhead *et al.* (2001) have cast doubt upon the status of

Hf as a truly fluid-immobile element; they see evidence in the New Britain subduction system for the transport of Hf in aqueous fluids when Nd is immobile. Their observations are based on the contrast in Hf isotope ratios of the mantle wedge beneath New Britain and the subducting crust of the Woodlark Basin. As we advocate an I-MORB composition for both the mantle wedge and the down-going subducted crust, any Hf mobility should have negligible impact on the Hf isotope ratio of the IVC magma source. Therefore, combined Nd and Hf isotope data can better document the source (mantle wedge) characteristics of the IVC lavas than combinations of isotope ratios involving $^{87}Sr/^{86}Sr$ isotope data (e.g. Pearce *et al.*, 1999). IVC lavas display a restricted range in $^{143}Nd/^{144}Nd$ and especially $^{176}Hf/^{177}Hf$ and lie within the Hf isotope range of I-MORB. Lavas from other Javan volcanoes diverge further from typical mantle (MORB) values towards more 'crustal' Hf–Nd isotopic compositions. Therefore, although the major element data indicate that the IVC lavas are moderately fractionated and are not primary magmas, the IVC source appears to be among the least affected by crustal inputs from either the slab or arc lithosphere (noting that the Hf isotope database is slightly more limited in comparison with Sr–Nd isotope data available). Volcanic rocks from the IVC and other volcanic centres on Java lie above the dividing line that separates MORB of Indian and Pacific provenance drawn in Hf–Nd isotope space by Pearce *et al.* (1999) (Fig. 6b), implying derivation from an I-MORB-like mantle source rather than a source similar to Pacific MORB, and corroborating conclusions from ratios of immobile trace elements (above).

In summary, restricted variation in isotope ratios and immobile trace element ratios suggests that the mantle sources of the different groups of IVC magmatic rocks are not distinct from each other. The mantle wedge beneath East Java is relatively fertile compared with that of many other island arcs, with HFSE (especially Nb and Ta) and HREE concentrations similar to those in the source of I-MORB.

Identification of subduction zone components: trace element constraints

Enrichment of LILE and LREE relative to HFSE in arc volcanic rocks has long been attributed to slab involvement (Hawkesworth *et al.*, 1979; Kay, 1980; White & Dupré, 1986; Davidson, 1987; McCulloch & Gamble, 1991), but there remains considerable uncertainty as to the source of this contribution (altered oceanic crust or sediments or both) and the transfer mechanism of this component to the sub-arc mantle (as a fluid or melt or both).

Th and the LREE are thought to be less mobile in aqueous fluids than the LILE (Tatsumi *et al.*, 1986; Pearce *et al.*, 1999) and, consequently, high Ce/Pb and Th/Yb ratios in arc lavas are taken to indicate a sedimentary contribution from the slab (Woodhead *et al.*, 2001; Gertisser & Keller, 2003). The large contrast in Ce/Pb and Th/Yb ratios between MORB (N- and I-MORB) and Indian Ocean sediments near Java (Table 6; Fig. 13a), suggests that relatively low Ce/Pb (3–7) and high Th/Yb (1–4) ratios of the IVC could be attributed to a sediment component in the arc mantle source. However, the slightly higher Th/Yb ratios observed in lavas of the low-Ca group suggest that this ratio was also affected by fractional crystallization. A plot of Th/Yb vs MgO (Fig. 13b) reveals slight elevation and correlation of Th/Yb ratios in the IC group compared with the CR group. The CR group displays limited variation (Th/Yb ~1·5) over the entire range of MgO, and we infer that this ratio is representative of the IVC source.

Elevations of LILE/LREE ratios in arc lavas compared with MORB are thought to indicate fluid addition to the mantle wedge from dehydration of the subducting slab (Ben Othman *et al.*, 1989; Elliott *et al.*, 1997). The Ba/La (23–36) and Sr/Nd (16–44) ratios of the IVC lavas are

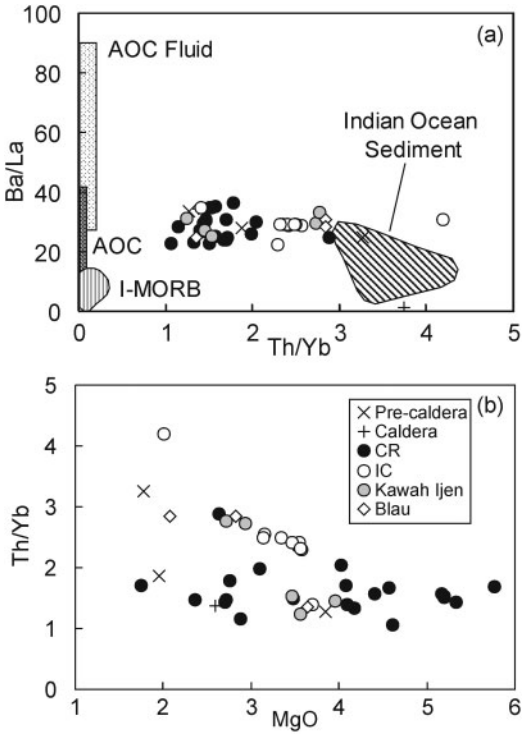

Fig. 13. (a) Ba/La–Th/Yb diagram highlighting the high Ba/La and Th/Yb ratios of IVC samples compared with I-MORB (Chauvel & Blichert-Toft, 2001). The field of Indian Ocean sediment is defined by three of the four sediment compositions used in the isotope mixing models in Fig. 14: bulk Java sediment (Plank & Langmuir, 1998), average terrigenous sediment (V33-75, -77, -79) and nanno-ooze (Gasparon & Varne, 1998). Altered oceanic crust data from Staudigel *et al.* (1996). AOC fluid ratios were calculated using mobility data of Tatsumi *et al.* (1986) and show the significantly higher Ba/La ratios in an AOC fluid relative to bulk AOC. (b) Th/Yb vs MgO for IVC groups.

slightly to significantly higher than those of Indian Ocean sediment and also much greater than I-MORB (Table 6; Fig. 13a), indicating that slab fluids may also be added to the IVC mantle source, possibly from the altered oceanic crust (AOC). The Ba/La ratios of the IVC volcanic rocks are not as high as those observed in the Kermadec, Mariana and New Britain arcs, where the dominant slab input is thought to be a hydrous fluid (Woodhead *et al.*, 2001). However, the overall flux of hydrous fluid might be the same in all these arcs; the lower Ba/La in the IVC lavas could reflect the addition of La from a subducted sedimentary component.

Modelling slab input: constraints from radiogenic isotopes

Two-component model: I-MORB + bulk sediment. Figure 14 shows simple mixing between an I-MORB source and bulk sediment for a variety of Indian Ocean sediment end-members (Table 7). Mixing arrays involving three of the four end-member sediments (A–C; Mn nodule, nanno-ooze and average Java sediment, respectively) produce reasonable fits to the general range of Java volcanic rocks. Addition of 0·5–1% average bulk Java sediment (C; Plank & Langmuir, 1998) to I-MORB produces a curve that passes through the most isotopically primitive IVC volcanic rocks (Fig. 14), but that is highly oblique to the IVC array. The terrigenous–biogenic sediment end-member (D) has high Sr/Nd and produces a convex-up mixing trend in Sr–Nd isotope space when added to I-MORB mantle (Fig. 14). Bulk terrigenous–biogenic sediments are unlikely to dominate the sediment contribution to the mantle source of the IVC volcanic rocks. This is supported by sediment data collected from the Indian Ocean. Terrigenous sands and silts, such as turbidites, are present in the average composition of the sedimentary column subducted at the Java trench as described by Plank & Langmuir (1993), but are minor components compared with clay and siliceous ooze. Boreholes 211 and 261 of Deep Sea Drilling Project (DSDP) leg 22 (SEATAR, 1981: http://www.ngdc.noaa.gov/mgg/geology/seatar.html) located in the Indian Ocean crust south of Java are dominated by nanno-ooze, nanno-claystone, a small amount of volcanic ash and a 12 cm thick surface layer of small manganese nodules.

Two-stage, three-component model: I-MORB + AOC component + bulk sediment. Two-component mixing fails to provide a good fit to the isotopic variation of the IVC lavas, suggesting that an additional isotopically distinct component is required in the source. Furthermore, some trace element ratios (e.g. Ba/La) are too high for MORB-source mantle and sediment mixtures to explain, but are consistent with a fluid contribution derived from the subducted AOC. Contributions from AOC have been inferred for many Sunda arc lavas (Turner & Foden, 2001) and there is considerable support for two separate contributions from the subducting slab to the mantle wedge in the petrogenesis of many other arc lavas (White & Patchett, 1984; Ellam & Hawkesworth, 1988; Thirlwall *et al.*, 1996; Elliott *et al.*, 1997; Hawkesworth *et al.*, 1997; Turner & Hawkesworth 1997; Turner *et al.*, 1997; Taylor & Nesbitt, 1998). Interaction of seawater with basalt produces significant chemical and isotopic changes (Hart *et al.*, 1974; White & Patchett, 1984). Altered oceanic crust displays a wide range in $^{87}Sr/^{86}Sr$ ratios whereas $^{143}Nd/^{144}Nd$ isotope ratios are generally indistinguishable from those of fresh

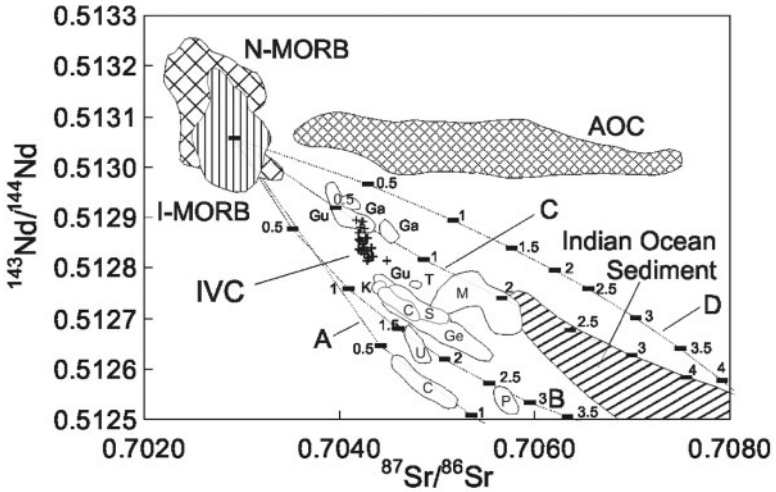

Fig. 14. $^{143}Nd/^{144}Nd$–$^{87}Sr/^{86}Sr$ diagram showing bulk mixing between I-MORB source (I-MORB*0·1, assuming 10% melting) and bulk sediment. Data sources for I-MORB, N-MORB, AOC and Indian Ocean sediment as in Fig. 6. Sediments used in mixing: A, Mn nodule; B, nanno-ooze; C, bulk Java sediment; D, terrigenous–biogenic. Sediment data sources and compositions are given in Table 7. Ticks along the mixing curves show the per cent of sediment in the mixture. Java field: Gu, Guntur; C, Cereme (Edwards, 1990); Ga, Galunggung (Gerbe *et al.*, 1992); S, Salak, Ge, Gede (this study); M, Merapi (Gertisser & Keller, 2001); K, Krakatau (Turner & Foden, 2001); T, Tangkuban Prahu, U, Ungaran, P, Papandayan (Whitford *et al.*, 1981).

Table 7: End-member compositions used in mixing calculations for Figs 14, 15 and 16

	Sr (ppm)	Nd (ppm)	Hf (ppm)	$^{87}Sr/^{86}Sr$	$^{143}Nd/^{144}Nd$	$^{176}Hf/^{177}Hf$
Fig. 14						
I-MORB source	13·5	0·97	0·25	0·702915	0·513042	0·283211
Sed A	857	187·9	5·73	0·709117	0·512236	0·282828
Sed B	126	51·9	–	0·71643	0·512228	–
Sed C	218	33·95	–	0·71682	0·51216	–
Sed D	398	15·36	–	0·708875	0·512411	–
Fig. 15						
FMM	22·42	0·697	–	0·704584	0·51307	–
Fig. 16						
IM1	13·9	1·02	0·25	0·702911	0·513044	0·283159
IM2	13·9	1·02	0·25	0·702819	0·513085	0·283124
IM3	13·9	1·02	0·25	0·70269	0·512991	0·283124
IM1 FMM	15·5	1·38	–	0·703502	0·513038	–
IM2 FMM	15·5	1·38	–	0·703422	0·513067	–
IM3 FMM	15·5	1·38	–	0·703309	0·513000	–

Mantle wedge represented by I-MORB source (I-MORB/10 assuming 10% melting). I-MORB data from Chauvel & Blichert-Toft (2001). Data sources: I-MORB average Sr concentration from Price *et al*. (1986), Rehkämper & Hofmann (1997) and Chauvel & Blichert-Toft (2001); I-MORB Nd and Hf concentration, Sr, Nd and Hf isotope data from Chauvel & Blichert-Toft (2001). Sediments: A, Mn nodule, V34-62 (White *et al.*, 1986; Ben Othman *et al.*, 1989); B, nanno-ooze, DSDP site 211 (Gasparon & Varne, 1998); C, average Java sediment (Plank & Langmuir, 1998); D, terrigenous–biogenic, average of V33-75, -77, -79 (Ben Othman *et al.*, 1989; Gasparon & Varne, 1998). FMM (fluid-modified mantle) mixture in Figs 15 and 16 is 3% AOC fluid and 97% I-MORB source. AOC end-member composition used in fluid calculation from Staudigel *et al*. (1995): Sr 67·32 ppm, Nd 13·08 ppm, $^{87}Sr/^{86}Sr$ 0·707437, $^{143}Nd/^{144}Nd$ 0·513023. Fluid created by 0·5% dehydration of AOC using $C_F = C_O/D + F^{(1-D)}$, where C_F is the concentration in the fluid, C_O is the concentration in AOC, D is the distribution coefficient given by Keppler (1996): Sr $D_{fluid/cpx} = 2{\cdot}1$, Nd $D_{fluid/cpx}$ estimated at 0·3 (relative to $D_{fluid/cpx}$ La = 1·0, Gd = 0·14 and Lu = 0·11) and F is the fraction of fluid created (0·005). I-MORB low $^{176}Hf/^{177}Hf$ sources: IM1 is MD37-05-02 (Chauvel & Blichert-Toft, 2001); IM2 is 54R-1, 115-121 (Nowell *et al.*, 1998); IM3 is MD34 D2 (Chauvel & Blichert-Toft, 2001).

MORB (Fig. 15). Because of the lack of isotopic data for altered Indian Ocean MORB we have used data for Atlantic MORB (Staudigel *et al.*, 1996) to consider the effect of adding this component to the mantle wedge. Regardless of how this component is added to the mantle wedge, either as a fluid (most commonly proposed; e.g. Ellam & Hawkesworth, 1988; Turner *et al.*, 1997) or melt (particularly where the subducting crust is young; e.g. Defant & Drummond, 1990), the isotopic composition of the resultant mixture will be generally the same; mixing I-MORB source with AOC fluid or melt will create a mixture with higher Sr isotope ratios and similar Nd isotope ratios to I-MORB. However, the quantity of AOC component required will be dependent on the transfer mechanism as a result of higher Sr/Nd ratios in fluids produced from the AOC compared with melts. The trajectory of the IVC data crosscuts any conceivable two-component mixing curve produced between the mantle source and an AOC–sediment mixture; therefore a two-stage model is preferred. In the mixing models, we have chosen to add the AOC component as a fluid, as it is hard to envisage (in a two-stage process whereby the mantle source is first contaminated by AOC prior to bulk addition of sediment; see Elliott *et al.*, 1997; Turner & Hawkesworth, 1997) melting of the AOC and addition of this to the mantle wedge without melting the sediments and incorporating them too, simultaneously, to the mantle wedge. Furthermore, the IVC lavas exhibit none of the geochemical traits thought to record slab melting (Defant & Drummond, 1990).

Figure 15 shows the results obtained from models of two-stage source contamination, where an I-MORB source is first contaminated by fluid from the AOC and then bulk sediment [Mn nodule (curve A-2) and nanno-ooze (curve B-2)]. These types of sediments are consistent with the findings from DSDP leg 22 boreholes 211 and 261 mentioned above. To create the fluid-modified mantle (FMM) component in this model, 3% AOC fluid was added (see Table 7 for AOC fluid calculation details). Mixing proportions of AOC and I-MORB are highly dependent on the Sr and Nd contents and isotopic ratios of AOC, which are themselves extremely variable. The fraction of fluid

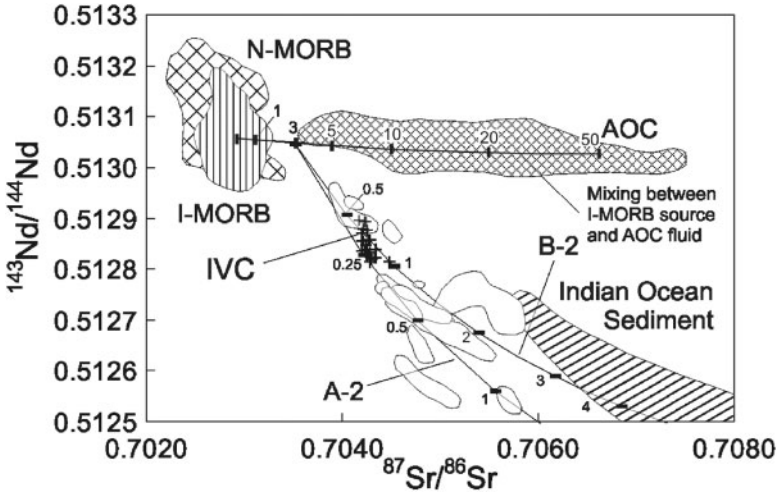

Fig. 15. $^{143}Nd/^{144}Nd$–$^{87}Sr/^{86}Sr$ diagram showing two-stage, three-component mixing. Data sources as in Figs 6 and 14. Mixing between I-MORB source and a fluid from the altered oceanic crust creates a mixture with higher $^{87}Sr/^{86}Sr$ and near identical $^{143}Nd/^{144}Nd$ to I-MORB source. Mixing of fluid-modified mantle with sediments A and B (as in Fig. 14) produces a good fit to the IVC data (curves A-2 and B-2, respectively). Tick marks indicate the per cent of sediment added to the fluid-modified mantle. End-member compositions and fluid calculations are given in Table 7.

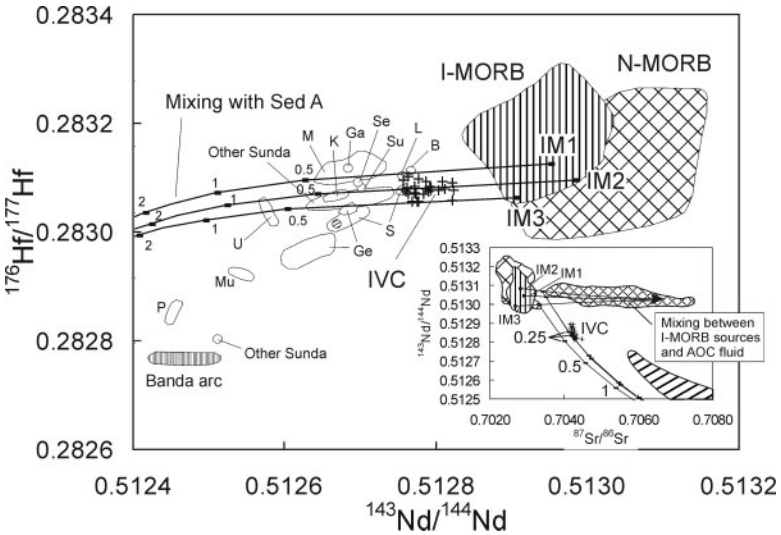

Fig. 16. $^{176}Hf/^{177}Hf$ vs $^{143}Nd/^{144}Nd$ showing mixing curves between three I-MORB source compositions with lower than average $^{176}Hf/^{177}Hf$ isotope ratios: IM1, IM2 and IM3 and sediment A (Mn nodule). Data sources as in Fig. 6. Java data: Merapi, Gede and Salak, this study; other Sunda: White & Patchett (1984); other named volcanoes [Mu, Muriah; L, Lamongan; B, Batur (Bali); Se, Semaru; Su, Sumbing; other abbreviations detailed in Fig. 6 caption] from Woodhead *et al.* (2001). End-member compositions are listed in Table 7. Inset diagram shows three-component mixing in Sr–Nd isotope space using the lower $^{176}Hf/^{177}Hf$ I-MORB source compositions used in the main diagram (rather than average I-MORB), AOC fluid (as in Fig. 15) and sediment A. The inset shows that using a lower $^{176}Hf/^{177}Hf$ I-MORB source composition has little effect on the shape of the mixing curve and the amount of sediment required when compared with curve A in Fig. 15, which uses average I-MORB source composition. Data fields as in Fig. 6 and end-member compositions are given in Table 7.

required is smaller if more highly altered basalt compositions are used, and greater if partial melting or bulk mixing of AOC is considered. The three-component models produce excellent fits not only to the trend of IVC lavas but also a large proportion of other Java volcanic rocks. Only a small percentage of sediment (0·25% Mn nodule or 0·5–1% nanno-ooze) is required to generate the isotopic values seen in the IVC volcanic rocks.

Three-component mixing in Nd and Hf isotope space. Modelling of two-stage source contamination in Nd–Hf isotope space is hampered by the paucity of Hf isotope data reported for altered oceanic crust. Nd isotope ratios remain relatively constant during hydrothermal and low-temperature seawater alteration of MORB, therefore, White & Patchett (1984) predicted that Hf isotope ratios will also be unaffected by the alteration of oceanic crust.

In these circumstances, contamination of the mantle source by a slab fluid from the AOC would be undetectable using Nd and Hf isotopes.

The relatively shallow array of IVC lavas projects back towards a mantle source with lower $^{176}Hf/^{177}Hf$ ratios than average I-MORB (Fig. 16). Mixing of an I-MORB source with a lower than average Hf isotope composition (IM1, IM2 and IM3; Table 7) with sediment A (Hf isotope data are unavailable for the nanno-ooze, B) produces mixing curves that correspond perfectly to the IVC data array, requiring <0·5% addition of sediment (all mixing curves in Fig. 16) and also match the percentage of sediment required to explain the IVC data in three-component Sr–Nd mixing (Fig. 15). Using low $^{176}Hf/^{177}Hf$ I-MORB source end-members instead of average I-MORB compositions does not affect the conclusions reached from three-component modelling in Sr–Nd isotope space (Fig. 16 inset); almost identical results are obtained (compare with curve A-2 in Fig. 15). This implies that, if a hydrous fluid is added to the mantle source from the altered oceanic crust, there is a minimal effect on the resulting Nd and Hf isotope ratios.

In conclusion, radiogenic isotope and trace element data for IVC lavas suggest that a three-component, two-stage source contamination model is applicable. In this model I-MORB mantle is metasomatized by slab fluids prior to addition of subducted sediment. Three-component models have also been suggested in geochemical studies of other island arc volcanoes (Ellam & Hawkesworth, 1988; Elliott *et al.*, 1997; Turner *et al.*, 1997; Taylor & Nesbitt, 1998). However, the order in which the two components from the slab (fluid and sediment) are introduced to the mantle wedge beneath IVC differs from that proposed in other models. The U-series isotopic compositions of Mariana lavas indicate that addition of a sedimentary component took place at least 350 kyr before fluid addition to the mantle wedge beneath the Mariana arc (Elliott *et al.*, 1997). The authors propose two possible models for the subduction component addition: (1) shallow (<120 km depth) sedimentary melts produce enriched sub-arc mantle, which is then dragged down to deeper depths where dehydration of the altered oceanic crust then releases fluid into the enriched sub-arc mantle causing melting; (2) altered oceanic crust dehydrates at shallow depth to produce hydrated peridotite mantle, which is down-dragged and dehydrates at around 120 km depth causing extensive melting. This material then encounters sedimentary material rising from greater depth. Elliot et al. (1997) acknowledge the inherent problems in their most simplified model (1) of satisfying thermal models of subduction zones (Peacock, 1991; Johnson & Plank, 1999). The reverse order in the addition of subduction components proposed at IVC (i.e. slab dehydration and fluid addition to the mantle wedge prior to sediment addition) appears mechanically more viable. However, in this model, fluid sourced predominantly from the oceanic crust must pass through the overlying sediment and avoid any sedimentary imprint. This is possible, as Elliott *et al.* (1997) pointed out that the sedimentary pile on top of the oceanic crust is likely to dehydrate and lose its fluid-mobile elements at shallower depths before major dehydration of the basaltic crust. This earlier fluid addition to the wedge may avoid being down-dragged to the region of arc magma genesis (Fryer, 1992) and, therefore, not contribute to magma geochemistry. Turner & Hawkesworth (1997) also proposed a model in which partial melts of sediment are added to the mantle wedge at relatively shallow levels prior to fluid addition from the slab. The timescale envisaged for fluid addition is of the order of 30–50 kyr before eruption.

In comparison, at volcanoes of the Andonara–Pantar section in the East Sunda arc, U-series, Sr–Nd–Pb isotope and trace element data support a similar transfer order for the addition of fluid- and sediment-sourced slab components (Hoogewerff *et al.*, 1997) as that proposed at IVC, although differing slightly in the exact nature of the slab components (sediment-derived hydrous fluid and siliceous melt). The hydrous fluid is proposed to dominate the input in the shallow part of the subduction zone, whereas the sedimentary melt dominates the flux at deeper levels. Evidence for relatively recent fluid addition is provided by ^{226}Ra excesses in volcanic rocks closest to the arc front in the Andonara–Pantar section and also in other Sunda arc lavas (Turner & Foden, 2001; Turner *et al.*, 2003).

Comparison of slab contributions

The amount of local sediment incorporated in the source region of IVC lavas (<0·5 Mn nodule or 0·5–1% nanno-ooze) is similar to or less than the amount of subducted sediment proposed in magma genesis at other arcs; for example, the Lesser Antilles (White & Dupré, 1986), Banda (Vroon, 1992), Izu–Bonin (Taylor & Nesbit, 1998) and Aleutian arcs (McCulloch & Perfit, 1981). Radiogenic isotopic compositions of other Sunda arc lavas are also accounted for by incorporation of similar amounts of subducted Indian Ocean sediment into the mantle wedge to that proposed beneath IVC: 1–2% (Merapi, Gertisser & Keller, 2003), <2% (general Sunda arc lavas, Turner & Foden, 2001), <5% (eastern Sunda arc, Stoltz *et al.*, 1990), 2·5% (Sangeang Api, East Sunda arc, Turner *et al.*, 2003). Several workers have proposed that the sedimentary component is added to mantle source in the form of a partial melt (Turner & Foden, 2001; Turner *et al.*, 2003). However, in eastern Sunda arc lavas calculated melt fractions of pelagic and biogenic sediments at low degrees of melting (1–10%) have low Sr/Nd ratios that produce curves that do not fit the volcanic data (even up to 40% melting) (Stoltz *et al.*, 1990). Sediment addition as a partial melt is a possibility beneath the IVC, but is not required to explain the data. However, considering this possibility we propose that the bulk sediment to mantle- or

fluid-modified mantle mixing curves provide an upper estimate of the amount of sediment contribution in the IVC magma source.

SUMMARY AND CONCLUSIONS

Differentiation processes can account for the spatial variations observed in the geochemistry of volcanic rocks at the Ijen Volcanic Complex. Major element and trace element modelling suggests that trends towards high CaO, Al_2O_3 and Sr contents with increasing MgO in the CR group (high-Ca group) and positive correlations of these elements in the IC group (low-Ca group) are a result of slight differences in fractionating mineral assemblages: olivine, clinopyroxene ± plagioclase fractionation dominating the CR group, and plagioclase > clinopyroxene and olivine in the IC group (Fig. 8). Spatial variations in lava geochemistry are controlled to some extent by subvolcanic structure. It is proposed that magma storage at shallower depths is prevented beneath volcanoes located on the caldera-rim (compare with the intra-caldera magmas) because of the presence of ring fractures, which focus and facilitate migration of magma towards the surface and inhibit the formation of shallow-level storage chambers. As a result, CR magmas do not undergo substantial shallow-level degassing or extensive plagioclase fractionation, like that envisaged for the IC volcanoes (Fig. 8). The linear orientation of the IC volcanoes further indicates the importance of sub-volcanic structure for volcanism at IVC. Location of Kawah Ijen at the intersection between the caldera rim and the northeastern edge of the intra-caldera lineation, combined with the eruption of lavas with the characteristics of both differentiation trends, implies that Kawah Ijen may be sourced by both the shallow and deep magma reservoirs by separate pathways (Fig. 8).

Low, mantle-like $\delta^{18}O$ values and a lack of correlation between isotope ratios and indices of differentiation imply that contamination by continental 'crustal' material is insignificant at IVC, consistent with IVC being located on thickened oceanic crust. Assimilation of isotopically indistinct material (i.e. older volcanic crust) cannot be discounted at IVC.

Despite the variation observed in major and trace element data, the HFSE ratios, Nd, Hf isotope ratios and $\delta^{18}O$ values of the IVC lavas are remarkably constant, suggesting that the subduction-modified mantle wedge source was relatively homogeneous. The IVC lavas have higher Hf and Nd isotope ratios than those of other Sunda arc volcanoes and lie on the edge of the I-MORB field in Hf–Nd isotope space, suggesting that they reflect the composition of the uncontaminated mantle wedge in East Java.

IVC magma genesis can be explained by two-stage, three-component source mixing. In this model, a fertile I-MORB source mantle wedge is infiltrated first by a hydrous slab fluid and then by sediment. As a result of the orientation of the IVC array and the shape of the mixing curves produced by different types of sediment addition in Hf–Nd isotope space (and constraints on sediment type from Sr–Nd isotope modelling), the I-MORB source component proposed has a lower than average $^{176}Hf/^{177}Hf$ isotope composition. In the model, the I-MORB source is contaminated by a small percentage of fluid created by the dehydration of the subducting slab (dominated by the chemistry of altered oceanic crust); this generates a mixture with higher $^{87}Sr/^{86}Sr$, and similar $^{143}Nd/^{144}Nd$ to I-MORB. At a later stage, less than 1% of Indian Ocean sediment is transferred from the slab into the fluid-modified mantle source. The type of subducted sediment proposed in magma genesis at IVC (nanno-ooze and Mn nodule) is consistent with those found as modern deposits on the sea bed south of East Java.

ACKNOWLEDGEMENTS

We thank John Gamble and Joel Baker for provision of IVC samples. Invaluable assistance was provided by Chris Ottley during trace element analysis and by Geoff Nowell throughout analytical work in the Arthur Holmes Isotope Geology Laboratory (AHIGL) at Durham University. We are grateful to D. Peate, I. Smith and R. Gertisser for constructive reviews, which greatly improved the manuscript. We also wish to thank Robert Hall and Helen Smyth of Royal Holloway University of London, and Val Troll and Jane Chadwick of Trinity College Dublin for their valuable comments and contributions. This work was funded by an NERC studentship (NER/S/A/2001/06127) and supported by the South East Asia Research Group (SEARG) at Royal Holloway University of London.

SUPPLEMENTARY DATA

Supplementary data for this paper are available at *Journal of Petrology* online.

REFERENCES

Ben Othman, D. B., White, W. M. & Patchett, J. (1989). The geochemistry of marine sediments, island arc magma genesis, and crust–mantle recycling. *Earth and Planetary Science Letters* **94**, 1–21.

Berlo, K. (2001). The magmatic evolution of the Ijen Caldera, East Java, Indonesia. Unpublished MSc. Thesis, University of Utrecht.

Brenan, J., Shaw, H. F., Phinney, D. L. & Ryerson, J. F. (1995). Mineral–aqueous fluid partitioning of trace elements at 900°C and 2·0 GPa: constraints on the trace element geochemistry of mantle and deep crustal fluids. *Geochimica et Cosmochimica Acta* **59**, 3331–3350.

Charlier, B. L. A., Ginibre, C., Morgan, D., Nowell, G. M., Pearson, D. G., Davidson, J. P. & Ottley, C. J. (2006). Methods for the microsampling and high-precision analysis of strontium and rubidium isotopes at single crystal scale for petrological and geochronological applications. *Chemical Geology* **232**, 114–133.

Chase, C. G. (1978). Plate kinematics: the Americas, East Africa, and the rest of the world. *Earth and Planetary Science Letters* **37**, 355–368.

Chauvel, C. & Blichert-Toft, J. (2001). A hafnium isotope and trace element perspective on melting of the depleted mantle. *Earth and Planetary Science Letters* **190**, 137–151.

Class, C., Miller, D. M., Goldstein, S. L. & Langmuir, C. H. (2000). Distinguishing melt and fluid subduction and components in Umnak volcanics, Aleutian Arc. *Geochemisty, Geophysics, Geosystems* **1**(6), paper number 20000601.

Davidson, J. P. (1987). Crustal contamination versus subduction zone enrichment: examples from the Lesser Antilles and implications for mantle source compositions of island arc volcanic rocks. *Geochimica et Cosmochimica Acta* **51**, 2185–2198.

Davidson, J. P. (1996). Deciphering mantle and crustal signatures in subduction zone magmatism. In: Bebout, G.E., Scholl, D.W., Kirby, S.H. & Platt, J.P. (eds) *Subduction: Top to Bottom. Geophysical Monograph, American Geophysical Union* **95**, 251–262.

Davidson, J. P., Dungan, M. A., Ferguson, K. M. & Colucci, M. T. (1987). Crust–magma interactions and the evolution of arc magmas: the San Pedro–Pellado volcanic complex, southern Chilean Andes. *Geology* **15**, 443–446.

Davidson, J. P., Hora, J. M., Garrison, J. M. & Dungan, M. A. (2005). Crustal forensics in arc magmas. *Journal of Volcanology and Geothermal Research* **140**, 157–170.

Defant, M. J. & Drummond, M. S. (1990). Derivation of some modern arc magmas by melting of young subducted lithosphere. *Nature* **347**, 662–665.

DeMets, C., Gordon, R. G., Argus, D. F. & Stein, S. (1990). Current plate motions. *Geophysical Journal International* **101**, 425–478.

Dowall, D. P., Nowell, G. M. & Pearson, D. G. (2003). Chemical preconcentration procedures for high-precision analysis of Hf–Nd–Sr isotopes in geological materials by plasma ionisation multi-collector mass spectrometry (PIMMS) techniques. In: Holland, G. & Tanner, S.D. (eds) *Plasma Source Mass Spectrometry. Special Publication, Royal Society of Chemistry*, pp. 321–337.

Edwards, C. M. H. (1990). Petrogenesis of tholeiitic, calc-alkaline and alkaline volcanic rocks, Sunda arc, Indonesia. PhD thesis, Royal Holloway, University of London.

Edwards, C. M. H., Menzies, M. A. & Thirlwall, M. F. (1991). Evidence from Muriah, Indonesia, for the interplay of supra-subduction zone and intraplate processes in the genesis of potassic alkaline magmas. *Journal of Petrology* **32**, 555–592.

Edwards, C. M. H., Morris, J. D. & Thirlwall, M. F. (1993). Separating mantle from slab signatures in arc lavas using B/Be and radiogenic isotope systematics. *Nature* **362**, 530–533.

Eiler, J. M., Crawford, A. J., Elliott, T. R., Farley, K. A., Valley, J. W. & Stolper, E. M. (2000). Oxygen isotope geochemistry of oceanic-arc lavas. *Journal of Petrology* **41**, 229–256.

Elburg, M., van Bergen, M., Hoogewerff, J., Foden, J., Vroon, P., Zulkarnain, I. & Nasution, A. (2002). Geochemical trends across an arc–continent collision zone: magma sources and slab–wedge transfer processes below the Pantar Strait volcanoes, Indonesia. *Geochimica et Cosmochimica Acta* **66**, 2771–2789.

Ellam, R. M. & Harmon, R. S. (1990). Oxygen isotope constraints on the crustal contribution to the subduction-related magmatism of the Aeolian Islands, southern Italy. *Journal of Volcanology and Geothermal Research* **44**, 105–122.

Ellam, R. M. & Hawkesworth, C. J. (1988). Elemental and isotopic variations in subduction related basalts: evidence for a three component model. *Contributions to Mineralogy and Petrology* **98**, 72–80.

Elliott, T., Plank, T., Zindler, A., White, W. & Bourdon, B. (1997). Element transport from slab to volcanic front at the Mariana Arc. *Journal of Geophysical Research* **102**, 14991–15019.

Fryer, P. (1992). A synthesis of Leg 125 drilling of serpentine seamounts on the Mariana and Izu–Bonin forearcs. In: Fryer, P., Pearce, J.A., Stokking, L.B. et al. (eds) *Proceedings of the Ocean Drilling Program, Scientific Results, 125.* College Station, TX: Ocean Drilling Program, pp. 593–614.

Gamble, J., Woodhead, J., Wright, I. & Smith, I. (1996). Basalt and sediment geochemistry and magma petrogenesis in a transect from oceanic island arc to rifted continental margin arc: the Kermadec–Hikurangi Margin, SW Pacific. *Journal of Petrology* **37**, 1523–1546.

Gasparon, M. & Varne, R. (1998). Crustal assimilation versus subducted sediment input in west Sunda arc volcanics: an evaluation. *Mineralogy and Petrology* **64**, 89–117.

Gasparon, M., Hilton, D. R. & Varne, R. (1994). Crustal contamination processes traced by helium isotopes: examples from the Sunda arc, Indonesia. *Earth and Planetary Science Letters* **126**, 15–22.

Gerbe, M.-C., Gouraud, A., Sigmarsson, O., Harmon, R. S., Joron, J.-L. & Provost, A. (1992). Mineralogical and geochemical evolution of the 1982–1983 Galunggung eruption (Indonesia). *Bulletin of Volcanology* **54**, 284–298.

Gertisser, R. & Keller, J. (2003). Trace element and Sr, Nd, Pb and O isotope variations in medium-K and high-K volcanic rocks from Merapi Volcano, Central Java, Indonesia: evidence for the involvement of subducted sediments in Sunda Arc magma genesis. *Journal of Petrology* **44**, 457–489.

Giannetti, B. (2001). Origin of the calderas and evolution of Roccamonfina volcano (Roman Region, Italy). *Journal of Volcanology and Geothermal Research* **106**, 301–319.

Grove, T. L., Elkins-Tanton, L. T., Parman, S. W., Chatterjee, N., Muntener, O. & Gaetani, G. A. (2003). Fractional crystallization and mantle-melting controls on calc-alkaline differentiation trends. *Contributions to Mineralogy and Petrology* **145**, 515–533.

Hamilton, W. B. (1979). *Tectonics of the Indonesian Region. US Geological Survey, Professional Papers* **1078**.

Handley, H. K. (2006). Geochemical and Sr–Nd–Hf–O isotopic constraints on volcanic petrogenesis at the Sunda arc, Indonesia. PhD thesis, Durham University.

Harmon, R. S. & Gerbe, M. C. (1992). The 1982–83 eruption at Galunggung volcano, Java (Indonesia): oxygen isotope geochemistry of a zoned magma chamber. *Journal of Petrology* **33**, 585–609.

Hart, S. R., Erlank, A. J. & Kable, E. J. D. (1974). Sea floor basalt alteration: some chemical and Sr isotopic effects. *Contributions to Mineralogy and Petrology* **44**, 219–230.

Hawkesworth, C. J., O'Nions, R. K. & Arculus, R. J. (1979). Nd and Sr isotope geochemistry of island arc volcanics, Grenada, Lesser Antilles. *Earth and Planetary Science Letters* **45**, 237–248.

Hawkesworth, C. J., Hergt, J. M., Ellam, R. M. & McDermott, F. (1991). Element fluxes associated with subduction related magmatism. *Philosophical Transactions of the Royal Society of London, Series A* **335**, 393–405.

Hawkesworth, C. J., Turner, S. P., McDermott, F., Peate, D. W. & van Calsteren, P. J. (1997). U–Th isotopes in arc magmas: implications for element transfer from the subducted slab. *Science* **276**, 551–555.

Hickey-Vargas, R. (1998). Origin of the Indian Ocean-type isotopic signature in basalts form the Philippine Sea plate spreading centres: an assessment of local versus large-scale processes. *Journal of Geophysical Research* **103**, 20963–20979.

Hilton, D. R. & Craig, H. (1989). A helium isotope transect along the Indonesian archipelago. *Nature* **342**, 906–908.

Hoffmann-Rothe, A., Ritter, O. & Haak, V. (2001). Magnetotelluric and geomagnetic modelling reveals zones of very high electrical conductivity in the upper crust of Central Java. *Physics of the Earth and Planetary Interiors* **124**, 131–151.

Hoogewerff, J. A., van Bergen, M. J., Vroon, P. Z., Hertogen, J., Wordel, R., Sneyers, A., Nasution, A., Varekamp, J. C., Moens, H. L. E. & Mouchel, D. (1997). U-series, Sr–Nd–Pb isotope and trace element systematics across an active island arc–continent collision zone: implications for element transfer at the slab–wedge interface. *Geochimica et Cosmochimica Acta* **61**, 1057–1072.

Ionov, D. A., Harmon, R. S., France-Lanord, C., Greenwood, B. & Ashchepkov, I. V. (1994). Oxygen isotope composition of garnet and spinel peridotites in the continental mantle: evidence from the Vitim xenolith suite, southern Siberia. *Geochimica et Cosmochimica Acta* **58**, 1463–1470.

Ito, E., White, W. M. & Gopel, C. (1987). The O, Sr, Nd and Pb isotope geochemistry of MORB. *Chemical Geology* **62**, 157–176.

Johnson, M. C. & Plank, T. (1999). Dehydration and melting experiments constrain the fate of subducted sediments. *Geochemistry, Geophysics, Geosystems* **1**, paper number 1999GC000014.

Kay, R. W. (1980). Volcanic arc magmas: implications of a melting–mixing model for element recycling in the crust–upper mantle system. *Journal of Geology* **88**, 497–522.

Kemmerling, G. L. L. (1921). Het Idjen Hoogland de geologie en geomorphologie van den Idjen. In: Kolff, G. et al (eds) de Koninklijke Natuurkundige Vereniging: Batavia,Weltevreden, 162 p.

Keppler, H. (1996). Constraints from partitioning experiments on the composition of subduction zone fluids. *Nature* **380**, 237–240.

Kessel, R., Schmidt, M. W., Ulmer, P. & Pettke, T. (2005). Trace element signature of subduction-zone fluids, melts and supercritical liquids at 120–180 km depth. *Nature* **437**, 724–727.

Macpherson, C. G. & Hall, R. (2001). Tectonic setting of Eocene boninite magmatism in the Izu–Bonin–Mariana forearc. *Earth and Planetary Science Letters* **186**, 215–230.

Macpherson, C. G. & Hall, R. (2002). Timing and tectonic controls in the evolving orogen of SE Asia and the western Pacific and some implications for ore generation. In: Blundell, D. J., Neubauer, F. & von Quadt, A. (eds) *The Timing and Location of Major Ore Deposits in an Evolving Orogen. Geological Society, London, Special Publication* **204**, 49–67.

Macpherson, C. G. & Mattey, D. P. (1998). Oxygen isotope variations in Lau Basin lavas. *Chemical Geology* **144**, 177–194.

Macpherson, C. G., Gamble, J. A. & Mattey, D. P. (1998). Oxygen isotope geochemistry of lavas from an oceanic to continental arc transition, Kermadec–Hikurangi margin, SW Pacific. *Earth and Planetary Science Letters* **160**, 609–621.

Macpherson, C. G., Hilton, D. R., Mattey, D. P. & Sinton, J. M. (2000). Evidence for an ^{18}O-depleted mantle plume from contrasting $^{18}O/^{16}O$ ratios of back-arc lavas from the Manus Basin and Mariana Trough. *Earth and Planetary Science Letters* **176**, 171–183.

Macpherson, C. G., Forde, E. J., Hall, R. & Thirlwall, M. F. (2003). Geochemical evolution of magmatism in an arc–arc collision; the Halmahera and Sangihe Arcs, eastern Indonesia. In: Larter, R. D. & Leat, P. T. (eds) *Intra-oceanic Subduction Systems: Tectonic and Magmatic Processes. Geological Society, London, Special Publication* **219**, 207–220.

Mandeville, C. W., Carey, S. & Sigurdsson, H. (1996). Magma mixing, fractional crystallisation and volatile degassing during the 1883 eruption of Krakatau volcano, Indonesia. *Journal of Volcanology and Geothermal Research* **74**, 243–274.

Mattey, D., Lowry, D. & Macpherson, C. (1994). Oxygen isotope composition of mantle peridotite. *Earth and Planetary Science Letters* **128**, 231–241.

McCulloch, M. T. & Gamble, J. A. (1991). Geochemical and geodynamical constraints on subduction zone magmatism. *Earth and Planetary Science Letters* **102**, 358–374.

McCulloch, M. T. & Perfit, M. R. (1981). $^{143}Nd/^{144}Nd$, $^{87}Sr/^{86}Sr$ and trace element constraints on the petrogenesis of Aleutian island arc magmas. *Earth and Planetary Science Letters* **56**, 167–179.

Münker, C., Worner, G., Yogodzinski, G. & Churikova, T. (2004). Behaviour of high field strength elements in subduction zones: constraints from Kamchatka–Aleutian arc lavas. *Earth and Planetary Science Letters* **224**, 275–293.

Nowell, G. M., Kempton, P. D., Noble, S. R., Fitton, J. G., Saunders, A. D., Mahoney, J. J. & Taylor, R. N. (1998). High precision Hf isotope measurements of MORB and OIB by thermal ionisation mass spectrometry: insights into the depleted mantle. *Chemical Geology* **149**, 211–233.

Nowell, G.M., Pearson, D.G., Ottley, C.J., Schweiters, J. & Dowall D. (2003). Long-term performance characteristics of a plasma ionisation multi-collector mass spectrometer (PIMMS): the ThermoFinnigan Neptune. In: Holland, G. & Tanner, S.D. (eds) Plasma Source Mass Spectrometry. Spec. Pub. *Royal Society of Chemistry*, 307–320.

Ottley, C. J., Pearson, D. G. & Irvine, G. J. (2003). A routine method for the dissolution of geological samples for the analysis of REE and trace elements via ICP-MS. In: Holland, G. & Tanner, S.D. (eds) *Plasma Source Mass Spectrometry. Special Publication, Royal Society of Chemistry*, pp. 221–230.

Patchett, P. J. (1983). Hafnium isotope results from mid-ocean ridges and Kerguelen. *Lithos* **16**, 47–51.

Patchett, P. J. & Tatsumoto, M. (1980). Hafnium isotope variations in oceanic basalts. *Geophysical Research Letters* **7**, 1077–1080.

Peacock, S. M. (1991). Numerical simulation of subduction zone pressure–temperature–time paths: constraints on fluid production and arc magmatism. *Philosophical Transactions of the Royal Society of London, Series A* **335**, 341–353.

Pearce, J. A. & Peate, D. W. (1995). Tectonic implications of the composition of volcanic arc magmas. *Annual Review of Earth and Planetary Sciences* **24**, 251–285.

Pearce, J. A., Kempton, P. D., Nowell, G. M. & Noble, S. R. (1999). Hf–Nd element and isotope perspective on the nature and provenance of mantle and subduction components in western Pacific arc–basin systems. *Journal of Petrology* **40**, 1579–1611.

Plank, T. & Langmuir, C. H. (1993). Tracing trace elements from sediment input to volcanic output at subduction zones. *Nature* **362**, 739–743.

Plank, T. & Langmuir, C. H. (1998). The chemical composition of subducting sediment and its consequences for the crust and mantle. *Chemical Geology* **145**, 325–394.

Potts, P. J., Tindle, A. G. & Webb, P. C. (1992). *Geochemical Reference Material Compositions: Rocks, Minerals, Sediments, Soils, Carbonates, Refractories and Ores Used in Research and Industry.* Caithness: Whittles Publishing.

Price, R. C., Kennedy, A. K., Riggs-Sneeringer, M. & Frey, F. A. (1986). Geochemistry of basalts from the Indian Ocean triple junction: implications for the generation and evolution of Indian Ocean ridge basalts. *Earth and Planetary Science Letters* **78**, 379–396.

Rehkämper, M. & Hofmann, A. W. (1997). Recycled ocean crust and sediment in Indian Ocean MORB. Earth. *and Planetary Science Letters* **147**, 93–106.

Reubi, O. & Nicholls, I. A. (2004). Magmatic evolution at Batur volcanic field, Bali, Indonesia: petrological evidence for polybaric fractional crystallisation and implications for caldera-forming eruptions. *Journal of Volcanology and Geothermal Research* **138**, 345–369.

Ringwood, A. E. (1974). The petrological evolution of island arc systems. *Journal of the Geological Society, London* **130**, 183–204.

Rotolo, S. G. & Castorina, F. (1998). Transition from mildly-tholeiitic to calc-alkaline suite: the case of Chichontepec volcanic centre. El Salvador, Central America. *Journal of Volcanology and Geothermal Research* **86**, 117–136.

Royse, K., Kempton, P. D. & Darbyshire, D. P. F. (1998). Procedure for the analysis for rubidium-strontium and samarium-neodymium isotopes at the NERC Isotope Geosciences Laboratory. *NERC Isotope Geosciences Laboratory Report Series* **121.**

Salters, V. J. M. (1996). The generation of mid-ocean ridge basalts from the Hf and Nd isotope perspective. *Earth and Planetary Science Letters* **141**, 109–123.

Salters, V. J. M. & Hart, S. R. (1991). The mantle sources of ocean islands and arc basalts: the Hf isotope connection. *Earth and Planetary Science Letters* **104**, 364–380.

Salters, V. J. M. & White, W. M. (1998). Hf isotope constraints on mantle evolution. *Chemical Geology* **145**, 447–460.

Sitorus, K. (1990). Volcanic stratigraphy and geochemistry of the Idjen Caldera Complex, East Java, Indonesia. MSc thesis, University of Wellington, New Zealand.

Smith, T. E., Thirlwall, M. F. & Macpherson, C. (1996). Trace element and isotope geochemistry of the volcanic rocks of Bequia, Grenadine Islands, Lesser Antilles Arc; a study of subduction enrichment and intra-crustal contamination. *Journal of Petrology* **37**, 117–143.

Smyth, H. (2005). Eocene to Miocene basin history and volcanic activity in East Java, Indonesia. PhD thesis, Royal Holloway University of London.

Staudigel, H., Davies, G. R., Hart, S. R., Marchant, K. M. & Smith, B. M. (1995). Large scale isotopic Sr, Nd and O isotopic anatomy of altered oceanic crust: DSDP/ODP sites 417/418. *Earth and Planetary Science Letters* **130**, 169–185.

Staudigel, H., Plank, T., White, B., & Schimincke, H.-U., (1996). Geochemical fluxes during seafloor alteration of the basaltic upper oceanic crust: DSDP Sites 417 and 418. In: Bebout, G.E., Scholl, D.W., Kirby, S.H. & Platt, J.P. (eds) *Subduction: Top to Bottom. Geophysical Monograph, American Geophysical Union* 96, 19–36.

Stille, P., Unruh, D. M. & Tatsumoto, M. (1986). Pb, Sr, Nd, and Hf isotopic constraints on the origin of Hawaiian basalts and evidence for a unique mantle source. *Geochimica et Cosmochimica Acta* **50**, 2303–2319.

Stolz, A. J., Varne, R., Davies, G. R., Wheller, G. E. & Foden, J. D. (1990). Magma source components in an arc–continent collision zone: the Flores–Lembata sector, Sunda arc, Indonesia. *Contributions to Mineralogy and Petrology* **105**, 585–601.

Stormer, J. C., Jr & Nicholls, J. (1978). XLFRAC; a program for the interactive testing of magmatic differentiation models. *Computers & Geosciences* **4**, 143–159.

Sun, S. & McDonough, W. F. (1989). Chemical and isotopic systematics of oceanic basalts: implications for mantle composition and processes. In: Saunders, A. D. & Norry, M. J. (eds) *Magmatism in the Ocean Basins. Geological Society, London, Special Publications* **42**, 313–345.

Tatsumi, Y., Hamilton, D. L. & Nesbitt, R. W. (1986). Chemical characteristics of fluid phase released from a subducted lithosphere and origin of arc magmas: evidence from high-pressure experiments and natural rocks. *Journal of Volcanology and Geothermal Research* **29**, 293–309.

Taylor, S. R. & McLennan, S. M. (1985). *The Continental Crust; its Composition and Evolution.*Oxford: Blackwell Scientific.

Taylor, R. N. & Nesbitt, R. W. (1998). Isotopic characteristics of subduction fluids in an intra-oceanic setting, Izu–Bonin Arc, Japan. *Earth and Planetary Science Letters* **164**, 79–98.

Taylor, R. N., Nesbitt, R. W., Vidal, P., Harmon, R. S., Auvray, B. & Croudace, I. W. (1994). Mineralogy, chemistry, and genesis of the boninite series volcanics, Chichijima, Bonin Islands, Japan. *Journal of Petrology* **35**, 577–617.

Thirlwall, M. F. (1991). Long-term reproducibility of multicollector Sr and Nd isotope ratio analysis. *Chemical Geology; Isotope Geoscience Section* **94**, 85–104.

Thirlwall, M. F. & Graham, A. M. (1984). Evolution of high-Ca, high-Sr C-series basalts from Grenada, Lesser Antilles: the effects of intra-crustal contamination. *Journal of the Geological Society, London* **141**, 427–445.

Thirlwall, M. F., Graham, A. M., Arculus, R. J., Harmon, R. S. & Macpherson, C. G. (1996). Resolution of the effects of crustal assimilation, sediment subduction, and fluid transport in island arc magmas: Pb–Sr–Nd–O isotope geochemistry of Grenada, Lesser Antilles. *Geochimica et Cosmochimica Acta* **60**, 4785–4810.

Tregoning, P., Brunner, F. K., Bock, Y., Puntodewo, S. S. O., McCaffrey, R., Genrich, J. F., Calais, E., Rais, J. & Subarya, C. (1994). First geodetic measurement of convergence across the Java Trench. *Geophysical Research Letters* **21**, 2135–2138.

Turner, S. & Foden, J. (2001). U, Th and Ra disequilibria, Sr, Nd and Pb isotope and trace element variations in Sunda arc lavas: predominance of a subducted sediment component. *Contributions to Mineralogy and Petrology* **142**, 43–57.

Turner, S. & Hawkesworth, C. (1997). Constraints on flux rates and mantle dynamics beneath island arcs from Tonga–Kermadec lava geochemistry. *Nature* **389**, 568–573.

Turner, S., Hawkesworth, C., Rogers, N., Bartlett, J., Worthington, T., Hergt, J., Pearce, J. & Smith, I. (1997). ^{238}U–^{230}Th disequilibria, magma petrogenesis and flux rates beneath the depleted Tonga–Kermadec island arc. *Geochimica et Cosmochimica Acta* **61**, 4855–4884.

Turner, S., Foden, J., George, R., Evans, P., Varne, R., Elburg, M. & Jenner, G. (2003). Rates and processes of potassic magma evolution beneath Sangeang Api volcano, East Sunda Arc, Indonesia. *Journal of Petrology* **44**, 491–515.

van Bemmelen, R. W. (1949). *The Geology of Indonesia. Vol 1A*. The Hague: Government Printing Office.

van Bergen, M. J., Vroon, P. Z., Varekamp, J. C. & Poorter, R. P. E. (1992). The origin of the potassic rock suite from Batu Tara Volcano (East Sunda Arc, Indonesia). *Lithos* **28**, 261–282.

Vervoort, J. D., Patchett, P. J., Blichert-Toft, J. & Albarède, F. (1999). Relationships between Lu–Hf and Sm–Nd isotopic systems in the global sedimentary system. *Earth and Planetary Science Letters* **168**, 79–99.

Vroon, P. Z. (1992). Subduction of continental material in the Banda Arc, Eastern Indonesia: Sr–Nd-Pb isotope and trace-element evidence from volcanics and sediments. PhD thesis, University of Utrecht.

Vroon, P. Z., van Bergen, M. J., Klaver, G. J. & White, W. M. (1995). Strontium, neodymium, and lead isotopic and trace-element signatures of the East Indonesian sediments: provenance and implications for Banda Arc magma genesis. *Geochimica et Cosmochimica Acta* **59**, 2573–2598.

Vroon, P. Z., Lowry, D., van Bergen, M. J., Boyce, A. J. & Mattey, D. P. (2001). Oxygen isotope systematics of the Banda arc: low $\delta^{18}O$

despite involvement of subducted continental material in magma genesis. *Geochimica et Cosmochimica Acta* **65**, 589–609.

Wheller, G. E., Varne, R., Foden, J. D. & Abbott, M. J. (1987). Geochemistry of Quaternary volcanism in the Sunda–Banda Arc, Indonesia, and three-component genesis of island arc basaltic magmas. *Journal of Volcanology and Geothermal Research* **32**, 137–160.

White, W. M. & Dupré, B. (1986). Sediment subduction and magma genesis in the Lesser Antilles: isotopic and trace element constraints. *Journal of Geophysical Research* **91**, 5927–5941.

White, W. M. & Patchett, J. (1984). Hf–Nd–Sr isotopes and incompatible element abundances in island arcs: implications for magma origins and crustal–mantle evolution. *Earth and Planetary Science Letters* **67**, 167–185.

White, W. M., Patchett, J. & Ben Othman, D. (1986). Hf isotope ratios of marine sediments and Mn nodules; evidence for a mantle source of Hf in seawater. *Earth and Planetary Science Letters* **79**, 46–54.

Whitford, D. J. (1975). Strontium isotopic studies of the volcanic rocks of the Sunda arc, Indonesia, and their petrogenesis. *Geochimica et Cosmochimica Acta* **39**, 1287–1302.

Whitford, D. J., White, W. M. & Jezek, P. A. (1981). Neodymium isotopic composition of Quaternary island arc lavas from Indonesia. *Geochimica et Cosmochimica Acta* **45**, 989–995.

Woodhead, J. D., Eggins, S. M. & Gamble, J. (1993). High field strength and transition element systematics in island arc and back-arc basin basalts: evidence for multi-phase melt extraction and depleted mantle wedge. *Earth and Planetary Science Letters* **114**, 491–504.

Woodhead, J. D., Hergt, J. M., Davidson, J. P. & Eggins, S. M. (2001). Hafnium isotope evidence for 'conservative' element mobitiy during subduction processes. *Earth and Planetary Science Letters* **192**, 331–346.

You, C.-F., Castillo, P. R., Gieskes, J. M., Chan, L. H. & Spivack, A. J. (1996). Trace element behaviour in hydrothermal experiments: implications for fluid processes at shallow depths in subduction zones. *Earth and Planetary Science Letters* **140**, 41–52.